Report No. 4/2022

DOI: 10.4171/OWR/2022/4

Multiscale Coupled Models for Complex Media: From Analysis to Simulation in Geophysics and Medicine

Organized by
Malgorzata Peszynska, Corvallis
Iuliu Sorin Pop, Diepenbeek
Barbara Wohlmuth, Garching
Zohar Yosibash, Tel Aviv

23 January – 29 January 2022

ABSTRACT. Many real-life applications require mathematical models at multiple scales, defined in domains with complex structures, some of which having time dependent boundaries. Mathematical models of this type are encountered in seemingly disparate areas e.g., flow and deformation in the subsurface or beneath the ocean floor, and in processes of clinical relevance. While the areas are different, the structure of the models and the challenges are shared: the analysis and simulation must account for the evolution of the domain due to the many coupled processes in the multi-scale context. The key theme and focus of the workshop were novel ideas in the mathematical modeling, analysis, and numerical simulation, which are cross-cutting between the two application areas mentioned above. The talks have covered the mathematical treatment of such problems, as well as the development of efficent numerical discretization schemes and of solvers for large-scale problems.

Mathematics Subject Classification (2020): 35, 65, 74, 76, 86, 92.

Introduction by the Organizers

The workshop Multiscale coupled models for complex media has focused on the mathematical and numerical analysis of mathematical models encountered in clinical applications and the goesciences, and the efficent numerical simulation techniques. The unifying aspect was the mathematical structure, expressed thorugh coupled systems of (nonlinear) equation, modeling processes like flow, reactions

and mechanical deformation. These systems are defined in mixed-dimensional domains, or domains having a complex structure, with evolving interfaces at various scales.

The aim of this workshop was to identify relevant mathematical challenges connected with the types of models mentioned above, and in particular the appropriate mathematical and simulation tools. The programme included 21 lectures on the mathematical analysis, upscaling, numerical simulation and scientific computing of processes in clinical applications and geosciences, some of them having a survey character. In summary, the following topics were addressed:

- Mathematical methods for multiscale and mixed dimensional models, fluidstructure interactions, fractures (homogenization, Hibert/de Rham complexes, model order reduction);
- Computational methods, with sub-topics in isogeometric and higher order methods, immersed boundaries, generalized multiscale finite elements, machine learning, discontinuous Galerkin methods, domain decomposition;
- Advanced modelling concepts for clinical applications (ophtalomlogy, cardiovascular flows, biomechanics) and geosciences (energy and environment, sea ice, coastal waves).

The workshop benefited greatly of the participation of scientists with a broad and heterogeneous expertise, willing to collaborate and exchange ideas in a common mathematical language. The workshop was attended by 60 scientists (25 on site) from 17 countries in Europe, North America, Asia, and Australia, including 5 young scientists who regeived the generous support through the "Oberwolfach Leibniz Graduate Students" Programme.

The participants have experienced an inspiring and friendly atmosphere. There were many discussions, leading to promising initiatives. All participants are grateful for the outstanding professional support, the hospitality and the wonderful conditions offered by the MFO. The restrictions due to pandemic did not allow all participants to be present in person, but the institute has excellent facilities so that even those attending online could take part actively in discussions (either plenary, or in smaller groups during breaks), enjoy activities like a musical event, and, of course, give presentations.

Acknowledgement: The MFO and the workshop organizers would like to thank the National Science Foundation for supporting the participation of junior researchers in the workshop by the grant DMS-1641185, "US Junior Oberwolfach Fellows".

Workshop: Multiscale Coupled Models for Complex Media: From Analysis to Simulation in Geophysics and Medicine

Table of Contents

Ernst Rank (joint with Mohammed Elhaddad, Davide d'Angella, Lisa Hug, Stefan Kollmannsberger, Nina Korshunova, Z. Yosibash) Immersed Boundary Methods for Complex Media: Principles, Opportunities and Applications	175
Markus Gahn (joint with Willi Jäger, Maria Neuss-Radu) Rigorous derivation of coupled Stokes-Plate-Equations for fluid flow interacting with a thin porous elastic layer	176
Beatrice Riviere (joint with Rami Masri and Charles Puelz) Reduced Models for Blood Flows and Solute Transport in the Circulatory System	180
Giovanna Guidoboni Multiscale/multiphysics modeling: applications in ophthalmology and cardiology	183
Sunčica Čanić (joint with J. Kuan, L. Bociu, B. Muha, J. Webster) Some recent results on a deterministic, multi-layered, fluid-poroelastic structure interaction problem, and a stochastic fluid-structure interaction problem, motivated by biological applications	186
Eric Chung (joint with Yalchin Efendiev, Thomas Hou, Wing Tat Leung, Maria Vasilyeva, Mary Wheeler) Computational multiscale methods	189
Paola F. Antonietti (joint with Chiara Facciolà, Marco Verani) Discontinuous Galerkin approximation of flows in fractured porous media on polygonal and polyhedral grids	
Alessandro Veneziani (joint with Adrien Lefieux, Marina Piccinelli, Alessio Gizzi, Brad Leshnower, Habib Samady, Flavio Fenton) Cardiovascular Mathematics: Data, (Reduced) Models and Clinics	194
Martina Bukač (joint with Catalin Trenchea) Numerical methods for fluid - elastic/poroelastic structure interaction problems with biomedical applications	199
Ferdinando Auricchio (joint with coauthors) $Additive\ Manufacturing.\ A\ world\ full\ of\ opportunities\ and\ challenges!\ .\ .$	201
Alessandro Reali (joint with Alessia Patton) Some advances in isogeometric analysis of coupled and complex problems	201

Ricardo Ruiz-Baier (joint with Wietse M. Boon, Martin Hørnkjol, Miroslav Kuchta, Kent-André Mardal, Matteo Taffetani, Hans D. Westermeyer, Ivan Yotov)	
Mixed formulations for poroelasticity/free-flow using total pressure	203
Jan Martin Nordbotten (joint with Wietse M. Boon, Jon Eivind Vatne) A geometric approach to modeling, analysis, and numerics for fractured porous materials	206
John M. Stockie Multiscale modelling of maple sap flow	207
Alexander Popp (joint with Nora Hagmeyer, Matthias Mayr, Ivo Steinbrecher)	
Mixed-dimensional coupling of 1D geometrically exact beam finite elements and 3D continua for engineering applications	210
Clint Dawson (joint with Kazbek Kazhyken and Juha Videman) Discontinuous Galerkin Methods for Green-Naghdi Models Coupled with Geomorphology	212
Thi-Thao-Phuong Hoang Global-in-time Domain Decomposition Methods for Coupled Problems in Heterogeneous Porous Media	213
Fred Vermolen (joint with Qiyao Peng, Ginger Egberts, Wietse Boon) Agent-based and continuum-based mechanics in medical processes	216
Christoph Rettinger (joint with Ulrich Rüde, Bernhard Vowinckel) From Micro to Macro: Sediment Transport Simulations with a Fully Resolved Lattice Boltzmann - Discrete Element Method	219
Patrick Le Tallec (joint with Bertrand Leturcq) Reduced models for multiscale industrial structures: beyond homogeneization	221

Abstracts

Immersed Boundary Methods for Complex Media: Principles, Opportunities and Applications

Ernst Rank

(joint work with Mohammed Elhaddad, Davide d'Angella, Lisa Hug, Stefan Kollmannsberger, Nina Korshunova, Z. Yosibash)

Cutting a structure out of a larger body is a standard CAD-operation (typically associated with the term 'trimming') in geometric modelling. The reverse operation, i.e. immersing a computational in a 'fictitious domain' was suggested already in the 1960ies for a numerical approximation of boundary value problems. Yet only during the last decade, a unification of these two views of 'immersing' and 'trimming' in Immersed Boundary Methods (IBM) has been realized as an attractive possibility for closely integrating geometric modelling and numerical analysis. This contribution gives an introduction in the general principles of IBM and then concentrates on a specific variant, the Finite Cell Method (FCM), a combination of IBM with Isogeometric Analysis and Higher Order Finite Elements.

The major asset of IBM compared to classical boundary conforming Finite Element Methods applied to the solution of Partial Differential Equations is obvious: The physical domain of computation needs not be meshed into finite elements, which is, in particular in cased of complex three-dimensional geometries still a major issue for many applications. Instead of a mesh of boundary-conforming tetrahedra or hexahedra the simply shaped fictitious domain is devided into a Cartesian grid of uniform cells. On this grid an indicator function is defined, which characterizes points inside and outside the original physical body. The such defined grid is then used as a 'mesh' of cells, where each cell is treated like a finite element. The central advantage of saving the effort to generate a mesh yet comes with significant cost, and several critical questions need to be answered to obtain a feasible numerical method. First of all, cells cut by the boundary of the physical domain need special treatment in computation of element stiffness matrices and load vectors, as their integrand is discontinuous. We discuss several approaches, where space-tree based numerical integration is a simple and robust possibility. Another issue is the imposition of boundary conditions along segments which are not matching with edges of grid cells. There, Neumann and Dirichlet boundary conditions need to be applied in a weak sense. Simple penalty methods and more advanced Nitsche-type formulations can successfully be applied. Further consideration needs to be given to cells, which have only a small cut part interior to the physical domain. These may result in conditioning problems of the system matrix, which can yet be treated by suitable preconditioning techniques.

The Finite Cell Method extends these basic IBM principles in particular in two directions. Firstly, a p-extension of the shape functions resulting in a higher order approximation is applied, and secondly, an overlaid grid-refinement is developed.

This hierarchical hp-version of Immersed Boundary Methods shows excellent approximation properties, accuracy and efficiency. It can be demonstrated that even exponential rate of convergence is obtained in cases, where this optimal rate is observed for a boundary conforming p-extension.

After discussing these principles we then address the topic of connecting geometric models to analysis. This connection can be realised by evaluating the domain's indicator function, algorithmically by evaluating a Point Membership Test (PMT) for each integration point of the grid. While this PMT is the only necessary geometric information on the analysis side, it can be provided for all relevant types of geometric models by specifically taylored functionality. We show various examples, starting from CAD-models based on Constructive Solid Geometry, where the PMT is a combination of evaluations on geometric primitives and of Boolean operations. We then concentrate on image-based models as they result e.g. from Computer Tomography. For these models, voxel data can immediately be transfered to an extended PMT, which not only evaluates the domain's indicator function but also provided material properties at the point of consideration.

As fields of application of the presented FCM virtual material testing for additive manufacturing is addressed. We show examples on analysis of lattice structures, where we compare the mechanical properties of the 'as-designed' CAD-structure with the 'as-built' geometry obtained from Computer Tomography. Special emphasis is laid on a detailed validation of the developed methods. In the last part, a combination of FCM with phase field models applied to fracture problems in biomechanics and geomechanics is shown.

References

- [1] A. Düster, J. Parvizian, Z. Yang, E. Rank, The finite cell method for three-dimensional problems of solid mechanics, Comput. Methods Appl. Mech. Eng. 197 (2008).
- [2] L Hug, S Kollmannsberger, Z Yosibash, E Rank, A 3D benchmark problem for crack propagation in brittle fracture, Comput. Methods Appl. Mech. Eng. 364 (2020).
- [3] J. Jomo, O. Oztoprak, F. de Prenter, H. Zander, S. Kollmannsberger, E. Rank, Hierarchical multigrid approaches for the finite cell method on uniform and multi-level hp-refined grids, arXiv preprint arXiv:2010.00881 (2021)

Rigorous derivation of coupled Stokes-Plate-Equations for fluid flow interacting with a thin porous elastic layer

Markus Gahn

(joint work with Willi Jäger, Maria Neuss-Radu)

Flow and transport processes through complex porous media including thin structures play an important role in many real-life applications. A crucial example is the transport of substances from the lumen of blood vessels into the underlying biological tissue through the wall of the blood vessel consisting of several thin heterogeneous layers. The rigorous derivation of macroscopic models with effective interface laws between the different regimes plays an important role to reduce complexity of mathematical models without loss of essential factors. A famous

example is the law of Beavers-Joseph [2] which was derived rigorously in [11]. A stationary Stokes flow through an ϵ -periodic filter consisting of an array of (disconnected) obstacles is treated in [14] and [6, 7], and for small obstacles in [1]. While there are a lot of results concerning dimension reduction for thin elastic structures, see [4, 5] for the homogeneous case, [3] for oscillating coefficients, and [10] for perforated layers, rigorous results treating fluid flow through thin porous elastic layers seem to be missing in the literature.

In this talk we consider the fluid flow over a thin porous elastic layer Ω^M_ϵ separating two fluid-filled bulk domains Ω^+_ϵ and Ω^-_ϵ . The layer consists of a fluid part $\Omega^{M,f}_\epsilon$ and an elastic solid part $\Omega^{M,s}_\epsilon$. Thickness and periodicity of the layer are of order ϵ , where the parameter ϵ is small compared to the size of the bulk domains. The aim is the derivation of effective interface conditions between the bulk domains for $\epsilon \to 0$, when the thin layer reduces to an interface Σ . The micro-model is given by the following fluid-structure interaction problem: The fluid velocity $v_\epsilon = (v_\epsilon^+, v_\epsilon^M, v_\epsilon^-)$ and the fluid pressure $p_\epsilon = (p_\epsilon^+, p_\epsilon^M, p_\epsilon^-)$ are given by the instationary Stokes-equations

$$\begin{split} \partial_t v_\epsilon^\pm - \nabla \cdot D(v_\epsilon^\pm) + \nabla p_\epsilon^\pm &= f_\epsilon^\pm & \text{in } (0,T) \times \Omega_\epsilon^\pm, \\ \frac{1}{\epsilon} \partial_t v_\epsilon^M - \frac{1}{\epsilon} \nabla \cdot D(v_\epsilon^M) + \frac{1}{\epsilon} \nabla p_\epsilon^M &= \frac{1}{\epsilon} f_\epsilon^M & \text{in } (0,T) \times \Omega_\epsilon^{M,f}, \\ \nabla \cdot v_\epsilon &= 0 & \text{in } (0,T) \times \Omega_\epsilon^f, \end{split}$$

where $D(v_{\epsilon})$ is the symmetric gradient, and the displacement u_{ϵ} is given by

$$\frac{1}{\epsilon} \partial_{tt} u_{\epsilon} - \frac{1}{\epsilon^3} \nabla \cdot \left(A_{\epsilon} D(u_{\epsilon}) \right) = 0 \qquad \text{in } (0, T) \times \Omega_{\epsilon}^{M, s}.$$

At the fluid structure interface Γ_{ϵ} in the thin layer we assume continuity of velocity and the normal stresses

$$v_{\epsilon}^{M} = \partial_{t} u_{\epsilon} \qquad \text{on } (0, T) \times \Gamma_{\epsilon},$$

$$\frac{1}{\epsilon} \left(-p_{\epsilon}^{M} I + D(v_{\epsilon}^{M}) \right) \cdot \nu = \frac{1}{\epsilon^{3}} A_{\epsilon} D(u_{\epsilon}) \cdot \nu \qquad \text{on } (0, T) \times \Gamma_{\epsilon}.$$

On the fluid-fluid interface between the layer and the bulk domains we also have continuity of the velocities and normal stresses. Further, on the lateral boundary we assume homogeneous Dirichlet boundary conditions, and on the top/bottom a zero normal stress condition (do-nothing boundary condition).

The existence and uniqueness of the weak solution $(v_{\epsilon}, p_{\epsilon}, u_{\epsilon})$ can be established by the Galerkin-method and standard energy estimates. Based on a priori estimates uniformly with respect to ϵ , we can pass to the limit $\epsilon \to 0$, using the method of two-scale convergence for thin heterogeneous layers [12, 13]. A main ingredient for these estimates is a Korn-inequality [9] for thin perforated layers with zero lateral boundary conditions. From general two-scale compactness results also derived in [9] we obtain the following convergences for the micro-solutions in the two-scale sense: There exist $u_0^3 \in H^1((0,T), H_0^2(\Sigma)) \cap H^2((0,T), L^2(\Sigma))$ and $\tilde{u}_1 \in H^1((0,T), H_0^1(\Sigma))^3$ with $\tilde{u}_1^3 = 0$, and $u_2 \in H^1((0,T), L^2(\Sigma, H_{\#}^1(Z)/\mathbb{R}))^3$,

in Ω^{\pm} .

such that up to a subsequence (for $\alpha = 1, 2$)

 $\partial_t v_0^{\pm} - \nabla \cdot \left(D(v_0^{\pm}) \right) + \nabla p_0^{\pm} = f_0^{\pm}$

$$\chi_{\Omega_{\epsilon}^{M,s}} \frac{u_{\epsilon}^{\alpha}}{\epsilon} \xrightarrow{t.s.} \chi_{Z^{s}} (\tilde{u}_{1}^{\alpha} - y_{3} \partial_{\alpha} u_{0}^{3}),$$

$$\chi_{\Omega_{\epsilon}^{M,s}} u_{\epsilon}^{3} \xrightarrow{t.s.} \chi_{Z^{s}} u_{0}^{3},$$

$$\frac{1}{\epsilon} \chi_{\Omega_{\epsilon}^{M,s}} D(u_{\epsilon}) \xrightarrow{t.s.} \chi_{Z^{s}} (D_{\bar{x}}(\tilde{u}_{1}) - y_{3} \nabla_{\bar{x}}^{2} u_{0}^{3} + D_{y}(u_{2})),$$

and same results are valid if we replace u_{ϵ} with $\partial_t u_{\epsilon}$, and the limit functions with their time derivatives. The fluid velocity and pressure in the layer fulfill

$$\chi_{\Omega_{\epsilon}^{M,f}} v_{\epsilon}^{M} \xrightarrow{t.s.} \chi_{Z^{f}}(0,0,\partial_{t}u_{0}^{3})^{T},$$

$$\chi_{\Omega_{\epsilon}^{M,f}} \partial_{t} v_{\epsilon}^{M} \xrightarrow{t.s.} \chi_{Z^{f}}(0,0,\partial_{tt}u_{0}^{3})^{T},$$

$$\chi_{\Omega_{\epsilon}^{M,f}} D(v_{\epsilon}^{M}) \xrightarrow{t.s.} \partial_{t} \tilde{u}_{1}(t,\bar{x}) - y_{3} \nabla_{\bar{x}} \partial_{t} u_{0}^{3}(t,\bar{x})$$

$$\chi_{\Omega_{\epsilon}^{M,f}} p_{\epsilon}^{M} \xrightarrow{t.s.} 0.$$

Passing to the limit $\epsilon \to 0$ in the micro-model, we obtain that the limit function $(v_0^{\pm}, p_0^{\pm}, \tilde{u}_1, u_0^3)$ is the unique weak solution of the macro-model [8]

$$\begin{split} \nabla \cdot v_0^{\pm} &= 0 & \text{in } \Omega^{\pm}, \\ v_0^{\pm} &= (0,0,\partial_t u_0^3)^T & \text{on } \Sigma, \\ -\nabla_{\bar{x}} \cdot \left(a^* D_{\bar{x}}(\tilde{u}_1) + b^* \nabla_{\bar{x}}^2 u_0^3 \right) &= 0 & \text{in } \Sigma, \\ \partial_{tt} u_0^3 + \nabla^2 : \left(b^* D_{\bar{x}}(\tilde{u}_1) + c^* \nabla_{\bar{x}}^2 u_0^3 \right) &= \int_{\mathcal{I}^t} f_0^{3,M} dy + \left([\![-D(v_0^{\pm}) + p_0^{\pm} I]\!] \nu \right)_3 & \text{in } \Sigma, \end{split}$$

We see that on the macro scale the bulk solution is still given by the instationary Stokes-equations. The fluid velocity is continuous at the interface Σ and equal to the velocity of the interface, whereas the tangential components vanish. The displacement is described by a time dependent plate equation with homogenized coefficients carrying information about the micro structure of the layer, and an additional stress term enforced from the bulk fluid. The convergence results imply that in the topology of the two-scale convergence the micro solutions in the layer can be approximated by

$$\begin{split} v^{M}_{\epsilon,\mathrm{app}}(t,x) &= \partial_{t}u^{3}_{0}(t,\bar{x})e_{3} + \epsilon \left[\partial_{t}\tilde{u}_{1}(t,\bar{x}) - \frac{x_{3}}{\epsilon}\nabla_{\bar{x}}\partial_{t}u^{3}_{0}(t,\bar{x})\right],\\ p^{M}_{\epsilon,\mathrm{app}}(t,x) &= 0,\\ u_{\epsilon,\mathrm{app}}(t,x) &= u^{3}_{0}(t,\bar{x})e_{3} + \epsilon \left[\tilde{u}_{1}(t,\bar{x}) - \frac{x_{3}}{\epsilon}\nabla_{\bar{x}}u^{3}_{0}(t,\bar{x})\right] + \epsilon^{2}u_{2}\left(t,\bar{x},\frac{x}{\epsilon}\right). \end{split}$$

We see that the approximation of the displacement and the fluid velocity up to order ϵ is given by a Kirchhoff-Love displacement. Further, the approximate fluid velocity in the layer $v_{\epsilon,\mathrm{app}}^M$ is equal to the time derivative of the first two terms in the approximate displacement $u_{\epsilon,\mathrm{app}}$. In other words, in this order of approximation the fluid does not transport substances transversal through the layer. Using a

formal asymptotic expansion, we expect that the second order-corrector for the fluid velocity differs from $\epsilon^2 \partial_t u_2$, but a rigorous proof is missing. The transversal flux through the porous layer is important in applications, even if it is small, since such small effects may have a relevant impact in long time scales. Therefore, it is an important problem to determine higher order corrector and also error estimates with respect to ϵ , which give quantitative predictions about the approximation.

In many applications, like for example transport through the wall of arterial blood vessels, it is important to take into account transport of substances and to consider multi-layers. The layers may differ in their properties, like thickness, heterogeneity, and biochemical processes within the layers. It is also necessary to investigate the influence of biochemical substances on the mechanical properties of the layers, leading to strongly coupled problems between the fluid-, solid-, and transport equations. Here there are still a lot of open questions concerning the analysis and also the modelling for such kind of problems.

- [1] G. Allaire. Homogenization of the Navier-Stokes equations in open sets perforated with tiny holes II: Non-critical sizes of the holes for a volume distribution and a surface distribution of holes. *Arch. Rational Mech. Anal.*, 113:261–298, 1991.
- [2] G. S. Beavers and D. D. Joseph. Boundary conditions at a naturally permeable wall. J. Fluid Mech., 30:197–207, 1967.
- [3] D. Caillerie and J. Nedelec. Thin elastic and periodic plates. Mathematical Methods in the Applied Sciences, 6(1):159-191, 1984.
- [4] P. G. Ciarlet. Mathematical Elasticity: Volume I: Three-dimensional elasticity. North-Holland, Amsterdam, 1988.
- [5] P. G. Ciarlet. Mathematical elasticity: Volume II: Theory of plates. Elsevier, Amsterdam, 1997.
- [6] C. Conca. Étude d'un fluid traversant une paroi perforeé I. Comportement limite près de la paroi. J. Math. pures et appl., 66:1–43, 1987.
- [7] C. Conca. Étude d'un fluid traversant une paroi perforeé II. Comportement limite loin de la paroi. J. Math. pures et appl., 66:45–69, 1987.
- [8] M. Gahn, W. Jäger, and M. Neuss-Radu. Derivation of a system of coupled Stokes and plate equations for fluid flow through a thin porous elastic layer. (Preprint: arXiv:2112.03583).
- [9] M. Gahn, W. Jäger, and M. Neuss-Radu. Two-scale tools for homogenization and dimension reduction of perforated thin layers: Extensions, Korn-inequalities, and two-scale compactness of scale-dependent sets in Sobolev spaces. Submitted (Preprint: arXiv:2112.00559).
- [10] G. Griso, L. Khilkova, J. Orlik, and O. Sivak. Homogenization of perforated elastic structures. J. Elast., 141:181–225, 2020.
- [11] W. Jäger and A. Mikelić. On the boundary conditions at the contact interface between a porous medium and a free fluid. Ann. Scuola Norm. Sup. Pisa Cl. Sci., 23:403–465, 1996.
- [12] S. Marušić and E. Marušić-Paloka. Two-scale convergence for thin domains and its applications to some lower-dimensional model in fluid mechanics. Asympt. Anal., 23:23–58, 2000.
- [13] M. Neuss-Radu and W. Jäger. Effective transmission conditions for reaction-diffusion processes in domains separated by an interface. SIAM J. Math. Anal., 39:687–720, 2007.
- [14] E. Sánchez-Palencia. Boundary value problems in domains containing perforated walls. In Nonlinear partial differential equations and their applications. College de France Seminar, volume 3, pages 309–325, 1982.

Reduced Models for Blood Flows and Solute Transport in the Circulatory System

BEATRICE RIVIERE

(joint work with Rami Masri and Charles Puelz)

Computer models of the whole blood circulatory system can be used as non-invasive tools for the understanding and prediction of the cardiovascular state of patients suffering from hypoplastic left heart syndrom [9, 3]. While a full three-dimensional model of blood flow and oxygen transport in the veinous and systemic arteries coupled with blood vessels in the heart and organs would provide a detailed description of the blood pressure, velocity and the oxygen concentration, it is also prohibitively computationally expensive. The use of reduced models (0D and 1D) allows for a simulation of the whole circulatory system while providing sufficiently accurate results [8].

We present conservative reduced models for coupled flow and solute transport in a blood vessel with radius R [1, 2, 5]. The unknowns are the scaled cross sectional area of the vessel, A, the momentum, Q, and the radial average concentration, C:

(1)
$$A = R^2, \quad Q = AU, \quad U = \frac{2}{R^2} \int_0^R r v_x dr.$$

We consider two choices for the axial velocity profile v_x : a no-slip axial velocity profile and a flat axial velocity profile.

Case: no-slip axial velocity profile

(2)
$$\frac{\partial A}{\partial t} + \frac{\partial Q}{\partial x} = 0,$$

(3)
$$\frac{\partial Q}{\partial t} + \alpha \frac{\partial}{\partial x} \left(\frac{Q^2}{A} \right) + \frac{A}{\rho} \frac{\partial p}{\partial x} = -2\pi \nu \frac{\alpha}{\alpha - 1} \frac{Q}{A},$$

(4)
$$\frac{\partial (AC)}{\partial t} + \frac{\partial (QC)}{\partial x} - \frac{(\alpha - 1)^2}{2\alpha(3\alpha - 2)D} \frac{\partial}{\partial x} \left(Q^2 \frac{\partial C}{\partial x} \right) = 0.$$

The parameter $\alpha > 1$ depends on the choice of the axial velocity profile: for instance, a parabolic profile (Poiseuille flow) corresponds to $\alpha = 4/3$ whereas a plug flow profile corresponds to $\alpha = 1.1$. It has been noted that a realistic blood velocity profile is closer to the plug flow profile than to the Poiseuille flow profile [7]. The coefficients D, ρ and ν are the diffusion, density and kinematic viscosity respectively.

Case: flat axial velocity profile

$$\frac{\partial A}{\partial t} + \frac{\partial Q}{\partial x} = 0,$$

(6)
$$\frac{\partial Q}{\partial t} + \frac{\partial}{\partial x} \left(\frac{Q^2}{A} \right) + \frac{A}{\rho} \frac{\partial p}{\partial x} = 0,$$

(7)
$$\frac{\partial (AC)}{\partial t} + \frac{\partial (QC)}{\partial x} = 0.$$

In both cases, a closure relation is needed for the pressure. We choose:

$$p = p_0 + \beta (A^{1/2} - A_0^{1/2}),$$

where β is a positive parameter, p_0 is a reference pressure for area equal to A_0 . Riemann invariants for (5)-(7) can be explicitly derived [4]; they are used in determining boundary conditions at junctions between incoming and outgoing vessels.

In patients with single ventricle hearts, the computational model couples the one-dimensional partial differential equations above with compartmental models (nonlinear ordinary differential equations) for the major organs and the heart (right atrium, right ventricle and two valves). Using electrical analogy, compartmental models (0D models) are constructed as circuits with resistor and capacitor elements. Organ bed models contain arterial $(C_{\rm art})$ and venous $(C_{\rm ven})$ compliances and resistances $(R_{\rm art}, R_{\rm ven})$. Pressures in the arteriole and venule compartments are related to pressures within the incoming and outgoing vessels by:

(8)
$$p_{\operatorname{art},k} - p_{\operatorname{art}} = Q_{\operatorname{art},k} R_{\operatorname{art},k}, \quad 1 \le k \le N_{\operatorname{in}},$$

(9)
$$p_{\text{ven}} - p_{\text{ven},k} = Q_{\text{ven},k} R_{\text{ven},k}, \quad 1 \le k \le N_{\text{out}}.$$

Pressure and flow between the arterial and venous sides of the organ satisfy the relations:

(10)
$$p_{\text{art}} - p_{\text{ven}} = Q_{\text{cap}} R_{\text{cap}}, C_{\text{art}} \frac{dp_{\text{art}}}{dt} = Q_{\text{art}} - Q_{\text{cap}}, C_{\text{ven}} \frac{dp_{\text{ven}}}{dt} = Q_{\text{cap}} - Q_{\text{ven}}.$$

Finally conservation of mass is enforced by

(11)
$$Q_{\text{art}} = \sum_{k=1}^{N_{\text{in}}} Q_{\text{art},k}, \quad Q_{\text{ven}} = \sum_{k=1}^{N_{\text{out}}} Q_{\text{ven},k}.$$

The model for the right heart (right atrium, interior valve, right ventricle and exterior valve) is also built from electrical analogy. The flow through one valve is driven by the pressure gradient and a smoothed Heaviside function.

An explicit time integrator is used to discretize the flow equations ((2)-(3) or (5)-(6)) whereas a locally implicity time integrator is used for handling the transport equation ((4) or (7)). The spatial discretization method is the discontinuous Galerkin method with the local Lax-Friedrichs flux for the hyperbolic term [6].

Figure 1 shows the momentum and concentration for a simulation using a network of 55 blood vessels. The solutions are obtained at the middle of the right

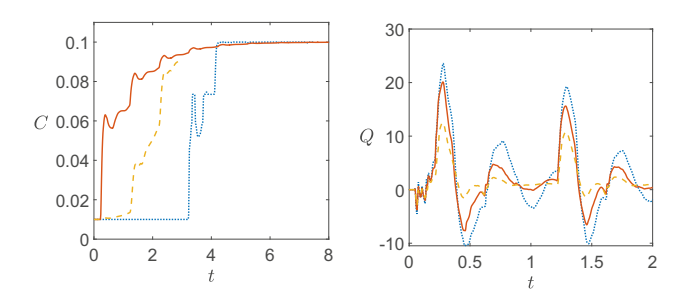


FIGURE 1. Flow (Q) and concentration (C) at the middle of the right femoral vessel as a function of time, for different axial velocity profiles. Axial velocity profiles are $\alpha = 4/3$ (red curve), $\alpha = 1.1$ (orange curve) and flat profile (blue curve).

femoral vessel. The length of that particular vessel is 44.4cm, the reference pressure is $p_0 = 75$ mmHg. The other parameters are: $A_0 = 0.139$ cm², $\beta = 2559000$ dyn/cm³. The red solid curve corresponds to $\alpha = 4/3$, the orange dashed line to $\alpha = 1.1$ and the dotted blue line is for the flat profile. The results indicate that the choice of the axial velocity profile may have a significant impact on the waveforms.

- A. Barnard, W. Hunt, W. Timlake, E. Varley, A theory of fluid flow in compliant tubes, Biophysical Journal 6 (1966), 717–724.
- [2] S. Čanić, E.H. Kim, Mathematical analysis of the quasilinear effects in a hyperbolic model blood flow through compliant axi-symmetric vessels, Mathematical Methods in the Applied Sciences 26 (2003), 1161–1186.
- [3] A.J. Chin, R.L. Watrous, Model-based comparison of the normal and Fontan circulatory systems part II: major differences in performance characteristics, World J. Pediatr. Congenit. Heart Surg. 6 (2015), 360–373.
- [4] L. Formaggia, D. Lamponi, A. Quarteroni, One-dimensional models for blood flow in arteries, J. Eng. Math. 47 (2003), 251–276.
- [5] R. Masri, C. Puelz, B. Riviere, A reduced model for solute transport in compliant blood vessels with arbitrary axial velocity profile, International Journal of Heat and Mass Transfer 176 (2021), 121379.
- [6] R. Masri, C. Puelz, B. Riviere, A discontinuous Galerkin method for blood flow and solute transport in one dimensional vessel networks, Communications on Applied Mathematics and Computation, (2021).
- [7] C.A. Owen, M. Roberts, Arterial vascular hemodynamics, Journal of Diagnostic Medical Sonography 23 (2007), 129–140.
- [8] C. Puelz, S. Acosta, B. Riviere, D. Penny, K. Brady, C.G. Rusin, A computational study of the Fontan circulation with fenestration or hepatic vein exclusion, Computers in Biology and Medicine 89 (2017), 405–418.
- [9] R.L. Watrous, A.J. Chin, Model-based comparison of the normal and Fontan circulatory systems part I: development of a general purpose, interactive cardiovascular model, World J. Pediatr. Congenit. Heart Surg. 5 (2014), 372–384.

Multiscale/multiphysics modeling: applications in ophthalmology and cardiology

Giovanna Guidoboni

When applied to the study of the human body, mathematical models must necessarily be *multiscale*, since phenomena occurring at small scales in space and time affect the macroscopic system behavior and viceversa, and *multiphysics*, since organ functions typically result from the complex interplay among fluid-dynamics, biomechanics and biochemistry [1]. The utilization of multiscale/multiphysics models to study living systems helps disentangle the interaction among coexisting (often competing) factors that is not possible to single out in experimental and clinical studies. Thus, multiscale/multiphysics models can serve as a virtual laboratory where multiple scenarios can be simulated, conjectures can be tested and new hypotheses can be formulated. In this work, two major applications of multiscale/multiphysics models are discussed, namely the study of glaucoma (Section 1) and the design of noninvasive sensors for cardiovascular monitoring (Section 2).

1. Modeling ocular physiology to preserve vision in glaucoma

Glaucoma is the leading cause of irreversible blindness worldwide and it involves progressive degeneration of the optic nerve and loss of retinal ganglion cells. An elevation of the pressure inside the eye (intraocular pressure, IOP) has been identified as a glaucoma risk factor since the mid-1800s and, to date, it remains the only approved therapeutic target for its treatment [2]. However, not all individuals with elevated IOP develop glaucoma and many glaucoma patients continue to progress to blindness despite successful IOP reduction. These patients account for as many as 1/3 of all glaucoma cases in the US, and yet a successful treatment strategy is not available for them. Abundant clinical and experimental evidence suggests that hemodynamic alterations are involved in the pathophysiology of glaucoma, but their relevance with respect to IOP remains controversial [3].

The main goal of this research is to help resolve this controversy by developing multiscale/multiphysics models to evaluate the relative importance of blood pressure (BP) and IOP in determining ocular perfusion and oxygenation, with the goal of identifying patient cohorts where vascular targets, in addition to IOP reduction, might be beneficial in preventing vision loss.

This research clarified, for the first time, that the pathological impact of IOP elevation on ocular hemodynamics does not depend solely on the IOP level but also on other patient-specific factors, such as blood pressure (BP). Our models provided specific ranges of combined BP and IOP values that would increase a patient's susceptibility to low perfusion and glaucomatous damage [4]. Our theoretical predictions have been recently confirmed by an independent population-based study involving nearly 10,000 individuals (nearly 20,000 eyes). Specifically, the Singapore Epidemiology of Eye Diseases study found that the association between low BP and glaucoma is especially pronounced in eyes with IOP \geq 21 mmHg, but not significant in eyes with IOP \leq 21 mmHg [5]. These findings have a huge impact

in glaucoma care, as they indicate that the concurrence of low BP and high IOP should be accounted for when stratifying glaucoma risk groups.

From the mathematical perspective, this project led to the first well-posedness analysis of deformable porous media models with nonhomogeneous boundary conditions [6] and the development of numerical methods that preserve, at the discrete level, the spatial fluxes of mass and linear momentum and the time evolution of the total energy in coupled systems of ordinary and partial differential equations [7, 8]. Current research directions include: (i) the well-posedness analysis for deformable porous media models with integral boundary conditions and their numerical solution, in order to address the multiscale coupling between three-dimensional models for tissue perfusion and lumped parameter models for systemic circulation; and (ii) the development of the first multiscale model for aqueous humor production and its pharmacological modulation, which entails the mathematical definition and numerical treatment of nontrivial multiscale connections among eye-level, cell-level and exchanger-level models.

2. Ballistocardiography for noninvasive cardiovascular monitoring

Cardiovascular diseases (CVDs) represent the first leading cause of death worldwide. Progression of a patient's CVD is often gradual and subtle. Early detection of CVD progression is crucial to intervene effectively, optimize a patient's treatment and mitigate negative outcomes. A noncontact approach to monitoring cardiovascular health is offered by ballistocardiography, whose signal, the ballistocardiogram (BCG), captures the repetitive motion of the center of mass of the human body resulting from the blood motion within the circulatory system. Interestingly, BCG-based monitoring of CVD does not require body contact and the signal reflects the status of the whole cardiovascular system. In the recent years, various technologies (e.g. piezoelectric sensors, load cells, accelerometers) have been utilized to design BCG sensors that can be placed under a bed mattress or in an armchair. Data show that BCG signals change with age and disease. However, to date, BCG signals lack a standardization, meaning that different BCG waveforms may be obtained for the same individual when utilizing different devices. The lack of standardization is the major obstacle currently hindering the use of BCG as a clinical diagnostic and monitoring instrument.

To overcome this challenge, we have developed a mathematical model capable of providing a quantitative characterization of signature changes in the BCG signal due to specific pathological cardiovascular conditions, such as reduced contractility of the left ventricle (as observed in systolic heart failure) and increased stiffness of the left ventricle (as observed in diastolic heart failure) [9, 10]. We are currently working on testing our model predictions on data collected on healthy subjects within the Center for Eldercare and Rehabilitation Technology directed by M. Skubic (College of Engineering, University of Missouri) [11], on critically ill patients within the Surgical Intensive Care Unit directed by Dr. Salman Ahmad (University of Missouri Health Care) [12], and on swine within the lab of Dr. Craig Emter (College of Veterinary Medicine, University of Missouri) [13].

- [1] R. Sacco, G. Guidoboni, A.G. Mauri, A comprehensive physically-based approach to modeling in bioengineering and life sciences, Academic Press, Elsevier (2019)
- [2] G. Guidoboni, A. Harris, R. Sacco (Eds), Ocular Fluid Dynamics. Anatomy, Physiology, Imaging Techniques, and Mathematical Modeling, Springer-Birkhauser, New York (2019)
- [3] A. Harris, G. Guidoboni, B. Siesky, S. Mathew, A. Verticchio-Vercellin, L. Rowe, and J. Arciero, Ocular blood flow as a clinical observation: value, limitations and data analysis, Progress in Retinal and Eye Research 78 (2020) 100841.
- [4] G. Guidoboni, A. Harris, S. Cassani, J. Arciero, B. Siesky, A. Amireskandari, L. Tobe, P. Egan, I. Januleviciene, and J. Park, *Intraocular pressure, blood pressure and retinal blood flow autoregulation: a mathematical model to clarify their relationship and clinical relevance*, Investigative Ophthalmology & Visual Science 55(7) (2014), 4105–4518.
- [5] Y. Tham, S. Lim, P. Gupta, T. Aung, T. Wong, and C. Cheng, Inter-relationship between ocular perfusion pressure, blood pressure, intraocular pressure profiles and primary open-angle glaucoma: the singapore epidemiology of eye diseases study, British Journal of Ophthalmology 102(10) (2018), 1402–1406.
- [6] L. Bociu, G. Guidoboni, R. Sacco, and J. Webster, Analysis of nonlinear poro-elastic and poro-visco-elastic models, Archive for Rational Mechanics and Analysis 222(3) (2016) 1445– 1519.
- [7] R. Sacco, A.G. Mauri, and G. Guidoboni, A stabilized dual mixed hybrid finite element method with Lagrange multipliers for three-dimensional problems with internal interfaces, Journal of Scientific Computing 82 (2020) 60.
- [8] L. Carichino, G. Guidoboni, and M. Szopos, Energy-based operator splitting approach for the time discretization of coupled systems of partial and ordinary differential equations for fluid flows: the Stokes case, Journal of Computational Physics 364(1) (2018) 235–256.
- [9] G. Guidoboni, L. Sala, M. Enayati, R. Sacco, M. Szopos, J. Keller, M. Popescu, L. Despins, V. Huxley, and M. Skubic, Cardiovascular function and ballistocardiogram: a relationship interpreted via mathematical modeling, IEEE Transactions on Biomedical Engineering 66(10) (2019) 2906–2917.
- [10] L.A. Despins, G. Guidoboni, M. Skubic, L. Sala, M. Enayati, M. Popescu, C.B. Deroche. Using sensor signals in the early detection of heart failure: A case study. Journal of Gerontological Nursing 46(7) (2020) 41–46.
- [11] N.M. Marazzi, G. Guidoboni, M. Zaid, L. Sala, S. Ahmad, L. Despins, M. Popescu, M. Skubic, J. Keller. Combining physiology-based modeling and evolutionary algorithms for personalized, non-invasive cardiovascular assessment based on electrocardiography and ballistocardiography. Frontiers in Physiology 12 (2021) Article 739035
- [12] M. Zaid, S. Ahmad, A. Suliman, M. Camazine, I. Weber, J. Sheppard, M. Popescu, M. Skubic, G. Guidoboni. Noninvasive cardiovascular monitoring based on electrocardiography and ballistocardio- graphy: a feasibility study on patients in the surgical intensive care unit. 43rd Annual International Conference of the IEEE Engineering in Medicine and Biology Society, October 31-November 4, 2021, Guadalajara, Mexico. Annu Int Conf IEEE Eng Med Biol Soc (2021) 951-954.
- [13] M. Zaid, L. Sala, J.R. Ivey, D.L. Tharp, C.M. Mueller, P.K. Thorne, S.C. Kelly, K.A. Santos Silva, A.R. Amin, P. Ruiz-Lozano, M.S. Kapiloff, L. Despins, M. Popescu, J. Keller, M. Skubic, S. Ahmad, C. Emter, G. Guidoboni. *Mechanism-driven modeling to aid noninvasive* monitoring of cardiac function via ballistocardiography. Frontiers in Medical Technology 4 (2022) Article 788264

Some recent results on a deterministic, multi-layered, fluid-poroelastic structure interaction problem, and a stochastic fluid-structure interaction problem, motivated by biological applications

SUNČICA ČANIĆ

(joint work with J. Kuan, L. Bociu, B. Muha, J. Webster)

The work reported here has been motivated by the design of lab-grown organs, such as a bioartificial pancreas. The design of lab-grown organs relies on using biocompatible materials, typically **poroelastic** hydrogels, to generate scaffolds to support seeded cells of different organs. Additionally, to prevent the patient's own immune cells from attacking the transplanted organ, the hydrogel containing seeded cells is encapsulated between two semi-permeable, nano-pore size membranes/plates and connected to the patient's vascular system via a tube (anastomosis graft). The semi-permeable membranes are designed to prevent the patient's own immune cells from attacking the transplant, while permitting oxygen and nutrients carrying blood plasma (Newtonian fluid) to reach the cells for long-term cell viability. A key challenge is to design a hydrogel with "roadways" for blood plasma to carry oxygen and nutrients to the transplanted cells [5].

1.1. Fluid-poroelastic structure interaction with a multi-layered poroelastic structure. The ability to mathematically model, analyze, and predict the behavior of biological and bioartificial tissue has never been more important. The related mathematical models are intrinsically multi-scale and multi-physics. Even at the mesoscale level, relevant to the understanding of the interplay between the architecture of poroelastic hydrogel matrix and blood flow, the current states of mathematical well-posedness and control theories are inadequate to address these questions. Continuum mechanics models of such systems are 3D fluid-3D structure interaction partial differential equations with moving interfaces. The relevant flow regimes necessitate the use of 3D viscous, incompressible flow models (the Navier-Stokes or time-dependent Stokes equations) coupled to 3D poroelasticity. To the best of our knowledge, there are only three manuscripts in the literature on fluidporoelastic structure interaction that address existence of solutions to this class of problems [2, 4, 1]. Critical issues arise for both the weak and strong PDE solutions, rooted in the well-known difficulties associated with the quasilinear problems in 3D (including the mathematical analysis of 3D Navier-Stokes and nonlinear Biot equations). Namely, for strong solutions, uniqueness of solutions can be obtained as well as appropriate smoothness of the interface, but these solutions are inherently local, precluding control and stability analysis on biological scales. On the other hand, weak solutions may exist for all times without smallness conditions, but they lack sufficient regularity for uniqueness, and they present issues associated with the regularity of the interface. Additionally, for the biological problems of interest here, the interface is, in fact, a poroelastic membrane or plate (the capsule), separating the "free fluid flow" in the anastomosis graft (tube) from the poroelastic gel (medium) containing the cells. To date, no comprehensive mathematical study of the resulting fluid-structure interaction problems involving such

multilayered poroelastic materials has been undertaken, and there is virtually no theory available. These **fluid-poroelastic structure interaction (FPSI) systems** are inherently challenging, and the addition of porosity as a central feature of the elastic structures, results in exceedingly complex mathematical models.

As a first step in developing a comprehensive mathematical theory involving existence, uniqueness, and control of solutions, as well as numerical methods development for physically-motivated 3D fluid-poroelastic systems arising in foundational biological design and control problems, we have recently studied the interaction between an incompressible, viscous fluid modeled by the **dynamic Stokes equation and a multilayered poroelastic structure** which consists of a thin, linear, poroelastic plate layer (in direct contact with the free Stokes flow) and a thick Biot layer. The fluid flow and the elastodynamics of the multilayered poroelastic structure are fully coupled across a **fixed** (linearized) interface through physical coupling conditions (including the Beavers-Joseph-Saffman condition), which present mathematical challenges related to the regularity of associated velocity traces.

In our recent work [1] we proved existence of weak solutions to this fluidstructure interaction problem with (i) a linear, dynamic Biot model, and (ii) a nonlinear quasi-static Biot component, where the permeability is a nonlinear function of the fluid content (as motivated by biological applications). The proof was based on constructing approximate solutions through Rothe's method, and using energy methods and a version of Aubin-Lions compactness lemma (in the nonlinear case) to recover the weak solution as the limit of approximate subsequences. We also provided uniqueness criteria and showed that constructed weak solutions are indeed strong solutions if one assumes additional regularity.

The next step will be to extend these results to nonlinear fluid-poroelastic structure interaction problems where the interface is moving, i.e., the problem is nonlinearly coupled. Additionally, including stochasticity in biological fluid-structure interaction is of great importance. In the next section we discuss a recent well-posedness result for a fluid-structure interaction problem with stochastic forcing.

1.2. Stochastic fluid-structure interaction. To capture the stochastic effects in biological fluid-structure interaction problems we recently studied a benchmark problem in which a stochastically forced linearly elastic membrane interacts with the flow of a viscous incompressible Newtonian fluid in two spatial dimensions. The membrane is modeled by the linear wave equation, and the fluid by the 2D time-dependent Stokes equations. The problem is forced by a "rough" stochastic forcing given by a time-dependent white noise $\dot{W}(t)$, where W is a given one-dimensional Brownian motion with respect to a complete probability space $(\Omega, \mathcal{F}, \mathbb{P})$ with complete filtration $\{\mathcal{F}_t\}_{t\geq 0}$. The forcing is applied to the "exterior" surface of the membrane. The fluid and the membrane are coupled via a two-way coupling describing continuity of fluid and structure velocities at the fluid-structure interface, and the continuity of contact force at the interface. The coupling is calculated at the linearized, fixed interface, rendering this problem a linear stochastic fluid-structure interaction problem. The goal was to show that despite the rough white noise, the resulting problem is well-posed, showing that

the underlying deterministic fluid-structure interaction problem is robust to noise. Indeed, in [3] we proved the existence of a unique weak solution in the probabilistically strong sense to this stochastic fluid-structure interaction problem. This means that there exist unique random variables (stochastic processes), describing the fluid velocity u, the structure velocity v, and the structure displacement η , such that those stochastic processes are adapted to the filtration $\{\mathcal{F}_t\}_{t\geq 0}$, i.e., they only depend on the past history of the processes up to time t and not on the future, which satisfy the weak formulation of the original problem almost surely.

In contrast to the deterministic case, the proof based on an operator splitting strategy presented in this work has several new interesting components:

- (1) The energy estimates are given in expectation, and do not necessarily hold pathwise. As a consequence, weak precompactness can be deduced only for the probability measures, or *laws* associated with approximate sequences, and not the sequences themselves.
- (2) The energy estimate has an extra term that accounts for the energy pumped into the problem by the stochastic forcing.
- (3) The operator splitting strategy must obey "the correct" order in which the operators associated with the deterministic and stochastic subproblems have to be "solved" so that the stochastic integrals containing the time increments of the stochastic forcing can be evaluated and bounded to produce a *stable scheme*.
- (4) To establish weak convergence of probability measures one must show that the probability measures are **tight**, which requires the use of a compactness result all Aubin-Lions even though the coupled problem is linear.
- (5) Once weak convergence of probability measures (laws) associated with approximate sequences is established, probabilistic techniques based on the Skorohod's theorem and Gyöngy-Krylov Lemma have to be employed to obtain an almost sure convergence to a weak solution.

To the best of our knowledge, this is the first well-posedness result for a stochastic FSI.

- L. Bociu, S. Čanić, B. Muha, and J. T. Webster. Multilayered poroelasticity interacting with stokes flow. SIAM Journal on Mathematical Analysis, Accepted 2021.
- [2] A. Cesmelioglu. Analysis of the coupled Navier-Stokes/Biot problem. Journal of Mathematical Analysis and Applications, 456(2):970-991, 2017.
- [3] J. Kuan, S. Čanić, Introduction to stochastic fluid-structure interaction Submitted 2022.
- [4] R. E. Showalter. Poroelastic filtration coupled to Stokes flow. In Control theory of partial differential equations, pages 243–256. Chapman and Hall/CRC, 2005.
- [5] S. Song, C. Blaha, W. Moses, J. Park, N. Wright, J. Groszek, W. Fissell, S. Vartanian, A. M. Posselt, and S. Roy. An intravascular bioartificial pancreas device (iBAP) with silicon nanopore membranes (SNM) for islet encapsulation under convective mass transport. *Lab* on a Chip, 17(10):1778–1792, 2017.

Computational multiscale methods

Eric Chung

(joint work with Yalchin Efendiev, Thomas Hou, Wing Tat Leung, Maria Vasilyeva, Mary Wheeler)

Many practical applications contain models with multiscale and high contrast coefficients. Due to scale disparity and the contrast, solving these problems using traditional approaches require very fine computational mesh, which are computationally expensive. Thus some type of coarse-grid models are necessary for these kinds of problems. The coarse grid does not necessarily resolve any scales and is typically much larger than the fine-grid size. Each coarse block typically contains many heterogeneities and high contrast. In modeling and simulations of multiscale problems, it is difficult to adjust coarse-grid sizes based on scales and contrast. Thus, it is important that the numerical performance is independent of these physical parameters, and depends only on the coarse grid size.

We have developed a systematic framework for multiscale model reduction using the Generalized Multiscale Finite Element Method (GMsFEM). The main idea is to construct multiscale basis functions in each coarse element via local spectral problems. The construction of the method begins with the snapshot space, which contains various potential modes of the solutions. Then local spectral problems are used to identify multiscale basis functions, which are dominant modes within the snapshot space. The goal of these constructions is to identify high-contrast and non-local features that need to be represented individually. These non-local features are typically channels (high-contrast regions that connect the boundaries of the coarse grid) and need separate (individual) basis functions. We note that the localizations of channels are not possible, in general, and this is the reason for constructing basis functions for channels separately. We remark that the local spectral problems and snapshots, if identified appropriately, correctly identify the necessary channels without any geometric interpretation. This makes the GMs-FEM a systematic tool for local multiscale model reduction. Adaptive GMsFEM is also developed to enrich multiscale spaces. See [1] for a review.

It is important that the error of the multiscale approximation depends only on the coarse grid size and is independent of the scales and contrast. The convergence of the GMsFEM depends on the eigenvalue decay, where the eigenvalues come from the local spectral problems. In order to design a multiscale method with a mesh-dependent convergence with a minimal number of basis functions, we propose the Constraint Energy Minimizing Generalized Multiscale Finite Element Method (CEM-GMsFEM) [2]. The convergence analysis of the GMsFEM suggests that one needs to include eigenvectors corresponding to small eigenvalues in the local spectral decomposition. We note that these small eigenvalues represent the channelized features, as we discussed above. For high-contrast problems, the local solutions do not decay in channels and thus, we need approaches that can take into account the information in the channels when constructing the decaying local solutions. Our proposed CEM-GMsFEM is able to tackle these challenges.

The above approaches are designed for linear multiscale problems, and their extension to nonlinear multiscale problems remains challenging. Many nonlinear problems have multiscale nature due to spatial and temporal scales. For example, the dynamics of multi-phase flow and transport in heterogeneous media varies over multiple space and time scales. There are in literature many successful linear and nonlinear upscaling tools. Nonlinear upscaling methods, e.g., known as pseudorelative permeability approach, computes nonlinear relative permeability functions based on single cell two-phase flow computations. It is known that these nonlinear approaches lack robustness and they are processes dependent. To overcome these difficulties, one needs better nonlinear upscaling methods. We have developed a new method called the Nonlinear Nonlocal Multi-continua Upscaling (NLNLMC) [3]. The goal of the method is to handle nonlinear multiscale problems with high contrast and non-separable scales.

The above introduced the NLNLMC method for nonlinear multiscale problems. The computations of the parameters in the upscaling model involve many local nonlinear problems, and are therefore computationally expensive. The main component of the NLNLMC method is the local downscaling functions, and these will give the parameters required in the final coarse grid equation. Given a set of macroscopic values, we will solve a local problem on an oversampling region to construct a fine scale downscaling function, whose mean values on coarse elements match the given macroscopic values. In general, this is an expensive task as these local problems are solved on-the-fly when the solution averages are given, and one cannot easily pre-compute these problems. This fact motivates the use of deep learning [4]. The main idea is to consider the macroscopic variables as input and the downscaling functions or their average values as output. Then suitable deep neural networks are trained and are used to approximate this expensive procedure. The resulting approach allows the use of deep neural network to learn the parameters required in the coarse scale equations. This can give a significant improvement in the computational times. We remark that using deep neural network for reduced models allows a robust learning process as there are fewer parameters

The research is partially supported by the Hong Kong RGC General Research Fund (Project numbers 14304719 and 14302620).

- [1] E. Chung, Y. Efendiev and T. Y. Hou, Adaptive multiscale model reduction with generalized multiscale finite element methods, Journal of Computational Physics 320 (2016), 69–95.
- [2] E. Chung, Y. Efendiev and W.T. Leung, Constraint energy minimizing generalized multiscale finite element method, Computer Methods in Applied Mechanics and Engineering 339 (2018), 298–319.
- [3] E. Chung, Y. Efendiev, W.T. Leung and M. Wheeler, Nonlinear nonlocal multicontinua upscaling framework and its applications, International Journal for Multiscale Computational Engineering 16 (2018), 487–507.
- [4] M. Vasilyeva, W.T. Leung, E. Chung, Y. Efendiev and M. Wheeler, Learning macroscopic parameters in nonlinear multiscale simulations using nonlocal multicontinua upscaling techniques, Journal of Computational Physics 412 (2020), 109323.

Discontinuous Galerkin approximation of flows in fractured porous media on polygonal and polyhedral grids

PAOLA F. ANTONIETTI

(joint work with Chiara Facciolà, Marco Verani)

We propose a unified formulation based on discontinuous Galerkin (dG) methods on polygonal/polyhedral grids for the simulation of flows in fractured porous media. Following [1], we first consider the case where the porous medium is cut by a single, non immersed fracture. We adopt a model for single-phase flows where the fracture Γ is modeled as a (d-1)-dimensional interface in a d-dimensional bulk domain $\Omega = \Omega_1 \cup \Omega$, cf. Figure 1, and model the flow in the porous medium and in the fracture by means of the Darcy's law. Following [1], we look for the bulk pressure p_i and velocity u_i , i = 1, 2 and the fracture pressure p_{Γ} and velocity u_{Γ} such that

$$\begin{array}{llll} \text{(1a)} & & \boldsymbol{u}_i = \boldsymbol{\nu}_i \nabla p_i & & & & \text{in } \Omega_i, & & i = 1, 2, \\ \text{(1b)} & & -\nabla \cdot \boldsymbol{u}_i = f_i & & & & \text{in } \Omega_i, & & i = 1, 2, \\ \text{(1c)} & & p_i = 0 & & & \text{on } \partial \Omega_i, & & i = 1, 2, \\ \text{(1d)} & & \boldsymbol{u}_{\Gamma} = \boldsymbol{\nu}_{\Gamma}^{\tau} \ell_{\Gamma} \nabla_{\tau} p_{\Gamma} & & & \text{in } \Gamma, \\ \text{(1e)} & & -\nabla_{\tau} \cdot \boldsymbol{u}_{\Gamma} = f_{\Gamma} + \llbracket -\boldsymbol{\nu} \nabla p \rrbracket & & & \text{in } \Gamma, \\ \text{(1f)} & & p_{\Gamma} = 0 & & & \text{on } \partial \Gamma, \\ \text{(1g)} & & -\{\boldsymbol{u}\} \cdot \mathbf{n}_{\Gamma} = \beta_{\Gamma} \llbracket p \rrbracket \cdot \mathbf{n}_{\Gamma} & & & \text{on } \Gamma, \\ \text{(1h)} & & & -\llbracket \boldsymbol{u} \rrbracket = \alpha_{\Gamma} (\{p\} - p_{\Gamma}) & & & \text{on } \Gamma. \end{array}$$

Here ν_i and f_i denote the restrictions of the bulk permeability tensor and of the source term to Ω_i , i=1,2, respectively, and \mathbf{n} is the outward unit normal vector to Ω . Analogously, ν_{Γ}^{τ} is the tangential component of the fracture's permeability, $\ell_{\Gamma} > 0$ is the fracture's thickness, $f_{\Gamma} \in L^2(\Gamma)$ is the source term, and ∇_{τ} and ∇_{τ} denote the tangential gradient and divergence operators, respectively. Finally, $\llbracket \cdot \rrbracket$ and $\lbrace \cdot \rbrace$ denote the jump and average operators, see [2], and β_{Γ} , α_{Γ} are chosen as in [1].

To introduce the unified dG formulation, we consider a polygonal/polyhedral mesh \mathcal{T}_h that is aligned with the fracture Γ , which is assumed to satisfy mild regularity assumptions, cf. [3]. We denote by \mathcal{F}_h the set of all its faces, that we can decompose in $\mathcal{F}_h = \mathcal{F}_h^I \cup \mathcal{F}_h^B \cup \Gamma_h$, where Γ_h is the set of faces belonging to the fracture and \mathcal{F}_i^I .

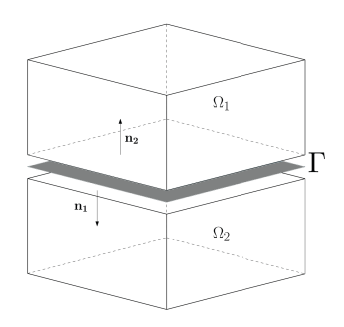


FIGURE 1. Sketch of the computational domain.

the set of faces belonging to the fracture and \mathcal{F}_h^I and \mathcal{F}_h^B are the sets of interior/boundary faces, respectively. The mesh \mathcal{T}_h . For given integers $k_E, k_F \geq 1$,

we introduce the finite-dimensional spaces:

$$\begin{aligned} Q_h^b &= \{q \in L^2(\Omega): \ q|_E \in \mathbb{P}_{k_E}(E) \ \forall E \in \mathcal{T}_h\}, \\ Q_h^\Gamma &= \{q_\Gamma \in L^2(\Gamma): \ q_\Gamma|_F \in \mathbb{P}_{k_F}(F) \ \forall F \in \Gamma_h\}, \end{aligned} \qquad \mathbf{W}_h^b = [Q_h^b]^d.$$

The discrete formulation is: Find $(p_h, \mathbf{u}_h, p_{\Gamma,h}, \mathbf{u}_{\Gamma,h}) \in Q_h^b \times \mathbf{W}_h^b \times Q_h^\Gamma \times \mathbf{W}_h^\Gamma$ s.t. (2)

$$\int_{\mathcal{T}_{h}} \mathbf{v}^{-1} \mathbf{u}_{h} \cdot \mathbf{v} = \int_{\mathcal{T}_{h}} \nabla p_{h} \cdot \mathbf{v} + \int_{\mathcal{F}_{h}^{I} \cup \Gamma_{h}} \{\widehat{p} - p_{h}\} \llbracket \mathbf{v} \rrbracket + \int_{\mathcal{F}_{h}^{I} \cup \mathcal{F}_{h}^{B} \cup \Gamma_{h}} \llbracket \widehat{p} - p_{h} \rrbracket \cdot \{ \mathbf{v} \},
\int_{\mathcal{T}_{h}} \mathbf{u}_{h} \cdot \nabla q - \int_{\mathcal{F}_{h}^{I} \cup \mathcal{F}_{h}^{B} \cup \Gamma_{h}} \{\widehat{\mathbf{u}}\} \cdot \llbracket q \rrbracket - \int_{\mathcal{F}_{h}^{I} \cup \Gamma_{h}} \llbracket \widehat{\mathbf{u}} \rrbracket \{q\} = \int_{\mathcal{T}_{h}} fq,
\int_{\Gamma_{h}} (\mathbf{v}_{\Gamma}^{\tau} \ell_{\Gamma})^{-1} \mathbf{u}_{\Gamma,h} \cdot \mathbf{v}_{\Gamma} = \int_{\Gamma_{h}} \nabla_{\tau} p_{\Gamma,h} \mathbf{v}_{\Gamma} + \int_{\mathcal{E}_{h,\Gamma}^{I}} \{\widehat{p}_{\Gamma} - p_{\Gamma,h}\} \llbracket \mathbf{v}_{\Gamma} \rrbracket + \int_{\mathcal{E}_{h,\Gamma}} \{\mathbf{v}_{\Gamma}\} \cdot \llbracket \widehat{p}_{\Gamma} - p_{\Gamma,h} \rrbracket,
\int_{\Gamma_{h}} \mathbf{u}_{\Gamma,h} \cdot \nabla_{\tau} q_{\Gamma} - \int_{\mathcal{E}_{\Gamma}^{I}} \{q_{\Gamma}\} \llbracket \widehat{\mathbf{u}}_{\Gamma} \rrbracket - \int_{\mathcal{E}_{\Gamma}^{I}} \{\widehat{\mathbf{u}}_{\Gamma}\} \cdot \llbracket q_{\Gamma} \rrbracket = \int_{\Gamma_{h}} \ell_{\Gamma} f_{\Gamma} q_{\Gamma} - \int_{\Gamma_{h}} \llbracket \mathbf{u} \rrbracket q_{\Gamma}$$

for all $(q_h, \mathbf{v}_h, q_{\Gamma,h}, \mathbf{v}_{\Gamma,h}) \in Q_h^b \times \mathbf{W}_h^b \times Q_h^\Gamma \times \mathbf{W}_h^\Gamma$. Here \hat{p} and $\hat{\mathbf{u}}$, \hat{p}_{Γ} and $\hat{\mathbf{u}}_{\Gamma}$ are the so called *numerical fluxes*, cf. [2]. A suitable definition of the *numerical fluxes* determine different dG methods.

Starting from (2) and suitably choosing the numerical fluxes, we discuss and analyze, in a unified setting, all the possible combinations of *primal-primal*, *mixed-primal*, *primal-mixed*, and *mixed-mixed* dG formulations for the bulk and fracture problems, respectively. For example, the *primal-primal* formulation follows from a suitable choice of the numerical fluxes $\hat{p} = \hat{p}(p_h)$, $\hat{\mathbf{u}} = \hat{\mathbf{u}}(p_h, p_{\Gamma,h})$, $\hat{p}_{\Gamma} = \hat{p}_{\Gamma}(p_{\Gamma,h})$, and $\hat{\mathbf{u}}_{\Gamma} = \hat{\mathbf{u}}_{\Gamma}(p_{\Gamma,h})$ and reads as

Find $(p_h, p_h^{\Gamma}) \in Q_h^b \times Q_h^{\Gamma}$ s.t. $\mathcal{A}_h ((p_h, p_h^{\Gamma}), (q, q_{\Gamma})) = \mathcal{L}_h(q, q_{\Gamma}) \ \forall (q, q_{\Gamma}) \in Q_h^b \times Q_h^{\Gamma}$, where $\mathcal{L}_h : Q_h^b \times Q_h^{\Gamma} \to \mathbf{R}$ is defined as $\mathcal{L}_h(q, q_{\Gamma}) = \int_{\mathcal{T}_h} fq + \int_{\Gamma_h} \ell_{\Gamma} f_{\Gamma} q_{\Gamma}$, and where $\mathcal{A}_h : (Q_h^b \times Q_h^{\Gamma}) \times (Q_h^b \times Q_h^{\Gamma}) \to \mathbf{R}$ is defined as

$$\mathcal{A}_h\left((p_h, p_h^{\Gamma}), (q, q_{\Gamma})\right) = \mathcal{A}_b(p_h, q) + \mathcal{A}_{\Gamma}(p_{\Gamma,h}, q_{\Gamma}) + \mathcal{C}((p_h, p_{\Gamma,h}), (q, q_{\Gamma})),$$

with

$$\mathcal{C}((p_h, p_{\Gamma,h}), (q, q_{\Gamma})) = \int_{\Gamma_h} \beta_{\Gamma} \llbracket p_h \rrbracket \cdot \llbracket q \rrbracket + \int_{\Gamma_h} \alpha_{\Gamma}(\{p_h\} - p_{\Gamma,h})(\{q\} - q_{\Gamma,h}).$$

and

$$\mathcal{A}_b^{\scriptscriptstyle P}(p_h,q) = \! \int_{\mathcal{T}_h} \! \boldsymbol{\nu} \nabla p_h \cdot \nabla q + \! \int_{\mathcal{F}_h^{\scriptscriptstyle I} \cup \mathcal{F}_h^{\scriptscriptstyle D}} \! \left(- \{ \boldsymbol{\nu} \nabla q \} \cdot [\![p_h]\!] - \{ \boldsymbol{\nu} \nabla p_h \} \cdot [\![q]\!] + \sigma_F [\![p_h]\!] \cdot [\![q]\!] \right),$$

$$\begin{split} \mathcal{A}_{\Gamma}(p_{\Gamma,h},q_{\Gamma}) &= \int_{\Gamma_{h}} \boldsymbol{\nu}_{\Gamma}^{\tau} \ell_{\Gamma} \nabla p_{\Gamma,h} \cdot \nabla q_{\Gamma} - \int_{\mathcal{E}_{\Gamma,h}^{I} \cup \mathcal{E}_{\Gamma,h}^{D}} \{\boldsymbol{\nu}_{\Gamma}^{\tau} \ell_{\Gamma} \nabla q_{\Gamma}\} \cdot \llbracket p_{\Gamma,h} \rrbracket \\ &- \int_{\mathcal{E}_{\Gamma,h}^{I} \cup \mathcal{E}_{\Gamma,h}^{D}} \{\boldsymbol{\nu}_{\Gamma}^{\tau} \ell_{\Gamma} \nabla p_{\Gamma,h}\} \cdot \llbracket q_{\Gamma} \rrbracket + \int_{\mathcal{E}_{\Gamma,h}^{I} \cup \mathcal{E}_{\Gamma,h}^{D}} \sigma_{e} \llbracket p_{\Gamma,h} \rrbracket \cdot \llbracket q_{\Gamma} \rrbracket. \end{split}$$

Here, σ_F and σ_e are suitable penalty functions to be properly defined. For all the possible combinations, we prove their well-posedness and derive a priori hp-version error estimates in a suitable (mesh-dependent) energy norm, [4, 3].

We also discuss the extension to networks of fractures. The key instrument here is the generalization of jump and average operators at fractures' intersection [5]. We assume that the fracture network is the union of N_{γ} fractures γ_k , each of which is a one co-dimensional manifold with zero curvature; see Fig. 2 for a two-dimensional example. At the fracture intersection \mathcal{I}_{\cap} our model is supplemented with suitable conditions. Let $\underline{b} = (b_1, b_2, \dots, b_{N_{\Gamma}})$ and $\underline{\mathbf{a}} = (\mathbf{a}_1, \mathbf{a}_2, \dots, \mathbf{a}_{N_{\Gamma}})$ be regular-enough scalar and vector-valued functions defined on the network. We introduce the following extension of jump and average operators for $\underline{\mathbf{a}}$ and \underline{b} at \mathcal{I}_{\cap} as

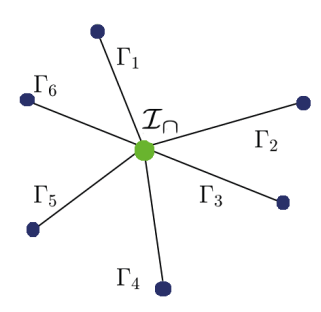


FIGURE 2. Example of $N_{\gamma} = 6$ fractures intersecting at \mathcal{I}_{Ω} for d = 2.

$$\begin{split} \{\underline{b}\}_{\cap} &= \frac{1}{N_{\Gamma}}(b_1 + b_2 + \dots + b_{N_{\Gamma}}), \qquad \{\underline{\mathbf{a}}\}_{\cap} = \frac{1}{N_{\Gamma}}\big(\mathbf{a}_i \cdot \boldsymbol{\tau}_i - \mathbf{a}_k \cdot \boldsymbol{\tau}_k\big)_{i,k \in \{1,2,\dots,N_{\Gamma}\},\, i < k}, \\ & [\![\underline{b}]\!]_{\cap} = \big(b_i - b_k\big)_{i,k \in \{1,2,\dots,N_{\Gamma}\},\, i < k}, \quad [\![\underline{\mathbf{a}}]\!]_{\cap} = \mathbf{a}_1 \cdot \boldsymbol{\tau}_1 + \mathbf{a}_2 \cdot \boldsymbol{\tau}_2 + \dots + \mathbf{a}_{N_{\Gamma}} \cdot \boldsymbol{\tau}_{N_{\Gamma}}, \end{split}$$

where trace operators on \mathcal{I}_{\cap} are understood. Based on the above definition we can extend our formulation so has to take into account networks of fracture. We prove its well-posedness as well as a priori hp-error estimates. Numerical experiments assess the theoretical error estimates and accuracy of the proposed formulations.

REFERENCES

- V. Martin, J. Jaffré, J. E. Roberts, Modeling fractures and barriers as interfaces for flow in porous media, SIAM J. Sci. Comput. 26 (2005), 1667–1691.
- [2] D. N. Arnold, F. Brezzi, B. Cockburn, L. D. Marini, Unified Analysis of Discontinuous Galerkin Methods for Elliptic Problems, SIAM J. Numer. Anal. 39 (2001/2002), 1749–1779.
- [3] P. F. Antonietti, C. Facciolà, M. Verani, Unified analysis of discontinuous Galerkin approximations of flows in fractured porous media on polygonal and polyhedral grids, Math. Eng. 2 (2020), 340–38.
- [4] P. F. Antonietti, C. Facciolà, M. Verani, A. Russo, Discontinuous Galerkin approximation of flows in fractured porous media on polytopic grids, SIAM J. Sci. Comput. 2 (2019), A109–A138.
- [5] P. F. Antonietti, C. Facciolà, M. Verani, Polytopic discontinuous Galerkin methods for the numerical modelling of flow in porous media with networks of intersecting fractures, Comput. Math. with Appl. (2021), 10.1016/j.camwa.2021.08.015

Cardiovascular Mathematics: Data, (Reduced) Models and Clinics

Alessandro Veneziani

(joint work with Adrien Lefieux, Marina Piccinelli, Alessio Gizzi, Brad Leshnower, Habib Samady, Flavio Fenton)

1. Introduction

"Cardiovascular mathematics" is a term introduced years ago [4] to denote the set of mathematical and numerical modeling techniques to specifically address cardiovascular diseases. Beyond the intrinsic speculative interest, one of the privileges of working in this area is the close contact with medical doctors and clinicians in what we can call "Clinical Cardiovascular Mathematics" (CCM). The potential and sometimes actual - role of rigorous mathematical and numerical modeling in the clinical practice significantly increase the appeal of this work.

This talk addresses some of the lessons learned working closely with clinicians on specific cardiovascular problems.

2. Some peculiarities of Clinical Cardiovascular Mathematics

Each of the subsequent subsections is inspired by a real clinical problem, but it gives room for some general conclusions and open challenges.

2.1. Models and Patient-specific Data: a potentially stormy relationship. As mathematicians, we love idealized models as a comfort zone where we can do (virtual) experiments without the burden of specific "2+ order" details. In CCM, unfortunately, "details" are called "patients". Any accurate quantitative analysis of blood flow with mathematical models requires patient-specific information; in particular, the "morphology" of the patient is critical [12]. Either level-set or machine learning techniques can be used for a (semi-)automated image processing that reconstructs the patient's morphology. But there is more.

Type B Aortic Dissection (TBAD) is a severe pathology where a part of the descending agree two lumens generated by a pocket in the regular wall that eventually leads to the formation of a parallel vessel (the false lumen - FL). The clinical decision of whether it is worth operating with surgery instead of medical treatment is currently guided by the patient's morphology. The distance between the Left Subclavian Artery and the Primal Intimal Tear (i.e., the main connection between the FL and the true lumen - PIT) is the landmark currently monitored. A large distance is considered a "no-growth" predictor, leading to drug treatment; a small distance suggests surgery. However, morphology is not enough in the cardiovascular system. We also have the "functionality", i.e., the bloodstream. We need to go beyond the image and simulate the blood. In an Emory patient presented with a large distance in 2006, we decided to perform a patient-specific simulation of the blood. This patient violated the clinical guideline, as the false lumen, in fact, grew significantly in 4 years. Our simulations [13] pointed out the role of the time-averaged Wall Shear Stress (TAWSS) in the FL: below a certain threshold, the TAWSS and the growth displayed a strong positive correlation. While this makes sense, we could not reproduce the same situation when working on more patients as the correlation growth/TAWSS was much more blurred and unclear. On the other hand, the 5-patient study displayed the role of the maximum wall shear stress at the PIT as a new landmark to categorize patients (Growth vs. No-Growth) [11]. To confirm this hypothesis, we are currently working on many more patients that will be regarded as the realization of a stochastic process to analyze with Principal Component Analysis, similarly to what was done in a previous project (Aneurisk) for cerebral aneurysms [9]. The take-home message is that each patient may tell a different story, computer-aided multi-patients clinical trials are mandatory in CCM. In turn, this leads to the need for (semi-)automated image processing systems as well as efficient numerical solvers to cope with a large number of patients within reasonable timelines.

2.2. Data and Model Assimilation: hybrid is good. Bioresorbable stents were introduced for young patients with acute coronary occlusions a few years ago. Despite the advantage of the complete absorption, they had several adverse effects in follow-up, to the point that they were withdrawn from the market. A possible hypothesis is that the abnormal thickness of the stent's struts (to stand the deployment pressure without a metallic core) triggers some blood recirculations that may induce new inflammations and, eventually, occlusions. As pointed out above, to test this hypothesis, we need to investigate many patient-specific geometries, and to have accurate functional data that may corroborate the hypothesis over a statistically significant number of patients. However, the automatic geometrical reconstruction of stented arteries is challenged by many aspects. Optical Coherence Tomography (OCT) generally obtains accurate images of stented coronaries, where it is possible to identify the struts with an excellent longitudinal resolution. However, these images are an internal view, in a frame moving with the catheter inside the vessel. The struts are detected only on a certain number of slices to form a point cloud. The identification of the underlying skeleton of the stent is not trivial. In addition, external imaging like angiographies are required to reconstruct the actual curvature of the vessel.

The stent skeletonization based on the point cloud was done by an innovative polyline-to-point cloud registration [8]. Using the undeployed stent as a template, we were able of automating the patient-specific skeletonization of the stent.

The merging of the two imaging techniques (OCT and angiographies) required the embedding of the OCT slices into a fictitious elastic domain that was deformed to match the coronary centerline reconstructed by the angiographies. This map was finally applied to the skeleton obtained by the registration. A physically-guided approach based on computational elasticity allowed then to extend the sparse information provided by the OCT into a 3D volume. After expanding the skeleton into a 3D structure using Nef-polyhedra and subtracting it to the unstented volume reconstructed by a standard level-set method, we are now able of reconstructing a stented artery for Computational Fluid Mechanics in a timeline of minutes (vs. days we needed a few years ago) [7]. The next step is the accurate

modeling of the stent erosion, which requires the definition of multiscale-in-time models.

The take-home message is that an accurate combination of data and models is the key for solving the most challenging problems in CCM: data and models together, and adequately merged, accomplished the mission.

2.3. Model Reduction: realtime model solution. Surgeons and clinicians in the operating room solve many "optimization problems" (generally constrained) by the help of some sparse data, experience, and intuition. As "optimization" is a well-established field of mathematics, it is natural to think that rigorous optimization techniques can be used for clinical problems. But, we have a but: computational time. Solving a shape-optimization problem constrained by the incompressible Navier-Stokes equations requires significant computational resources and time. A possible approach is to resort to purely data-driven methods. While this seems an appealing strategy, it is crucial to consider the massive amount of training data for strictly data-driven approaches. On the other hand, Model Order Reduction (MOR) has been established in the last few years as a rigorous approach for reducing computational costs in computational mechanics (and beyond). We have several different MOR approaches that can customize numerical solvers to specific problems with a tremendous reduction of computational costs. We illustrate hereafter some possible examples.

2.3.1. Snapshot-based model reduction. The Total Cavopulmonary Connection (TCPC) is a bridging surgery for newborn babies affected by the Hypoplasia of the Left Ventricle. It consists of an artificial connection between the Superior/Inferior Vena Cava with the Pulmonary Artery. The shape of this connection (or shunt) was related to some long-term effects in the patients [10]. While rigorous shape-optimization procedures are possible, the complexity of the geometry and of the flow in the TCPC prevented their use in the clinical practice.

Proper Orthogonal Decomposition (POD) is a procedure to reduce the computational complexity of some problems by creating an appropriate space of solutions that are determined by a relatively low number of degrees of freedom. Within an offline/online paradigm, one first creates a library of snapshots by solving the problem for a certain range of the parameters of interest (in our case, the ones underlying the geometrical definition); successively, the intrinsic redundancy of all the snapshots is filtered by extracting the singular values of the snapshot matrix and dropping the smallest ones. Finally, the solution of the online procedure (i.e., with new values of the parameters not considered Offline) is computed on the (relatively small) number of eigenvectors associated with the singular values retained at the previous stage. Consequently, we project the original problem on this subspace of eigenvectors, and solve it with a significant computational advantage.

In the shape optimization of the TCPC, where the flow distribution on the pulmonary artery must be optimized by the geometry, we need to resort to some iterative procedure to solve the Karush-Khun-Tucker equations associated with the problem. Each iteration requires solving the incompressible Navier-Stokes

equations in a cross-like domain. With a POD model reduction, each iteration can be accelerated to a fraction of seconds to make the entire procedure compatible with clinical timelines. This is an extremely hot and open research topic.

2.3.2. Non snapshot-based model reduction. In some cases, the singular values do not decay fast enough to guarantee an efficient model reduction unless the offline phase is guided by an accurate selection of the snapshots. In these cases, MOR not snapshot-based is possible.

A classical and challenging problem in cardiac electrophysiology is the optimal placement of the pace-maker leads or, in general, the optimal deployment of Cardiac Resynchronization Therapies (CRT). In this case too, iterative procedures underlying the optimization/data assimilation are generally computationally challenging. However, POD does not provide an adequate model reduction.

The Proper Generalized Decomposition (PGD) is a methodology based on an augmented variational formulation including all the parameters of interest as independent variables [3]. Numerically, this leads to Partial Differential Equations with many independent variables (much more than the classical four space-time variables). The numerical solution of this augmented problem can be accomplished by an iterative separation-of-variable approach in the so-called PGD Offline phase. At this point, the solution of the electrophysiology problem (the so-called Monodomain/Bidomain equations) for a new value of the parameters is a simple evaluation of the solution in the values specified by the parameters, with modest computational costs.

PGD was successfully applied to the variational data assimilation of the cardiac conductivities [1].

Another "reduced-modeling" approach for the solution of the incompressible Navier-Stokes equations in the arteries (i.e., cylindrical-like geometries) is represented by the so-called HiMOD [6]. HiMOD responds to the simple observation that, in arteries, the main dynamics occur along the centerline (axial direction). Therefore, the idea is to construct a customized method where one combines a classical 1D axial solution with some Fourier or polynomial spectral representation of the transversal solution. This reduces drastically the number of degrees of freedom of the solver with a tremendous computational advantage in pipes or networks of pipes. In this case, we do not have an Offline/Online paradigm, but just the construction of customized functional spaces that create a "psychologically 1D" blood flow solver. This can be used to manage time-consuming Uncertainty Quantification analyses of blood in a network of pipes [5].

The take-home message is that, contrarily to a popular idea, not only purely data-driven methods can be real-time, as reduced models can include physical conceptualizations of computational mechanics within a competitive timeline.

3. Conclusions

CCM is a fantastic place for advanced methods in applied mathematics, with many open problems and challenges. The potential impact of methods and tools on healthcare and society feeds the will to solve the most complex problems. It is essential that mathematicians drive the correct combination of models and data when facing these challenges. While it is now clear the potential disruption of data misinterpretations [2], quantitative and precision medicine can tremendously improve the fate of many patients, thanks to the unique opportunity offered by the data availability and the power of models and their reduction, to fit within the pressing clinical timelines. And this calls for the best mathematics we have.

The support of US NSF, Emory URC, and NIH is gratefully acknowledged.

- Alessandro Barone, Michele Giuliano Carlino, Alessio Gizzi, Simona Perotto, and Alessandro Veneziani. Efficient estimation of cardiac conductivities: A proper generalized decomposition approach. *Journal of Computational Physics*, 423:109810, 2020.
- [2] Carl T Bergstrom and Jevin D West. Calling bullshit: the art of skepticism in a data-driven world. Random House Trade Paperbacks, 2021.
- [3] Francisco Chinesta, Roland Keunings, and Adrien Leygue. The proper generalized decomposition for advanced numerical simulations: a primer. Springer Science & Business Media, 2013.
- [4] Luca Formaggia, Alfio Quarteroni, and Allesandro Veneziani. Cardiovascular Mathematics: Modeling and simulation of the circulatory system, volume 1. Springer Science & Business Media, 2010.
- [5] Sofia Guzzetti, LA Mansilla Alvarez, PJ Blanco, Kevin Thomas Carlberg, and A Veneziani. Propagating uncertainties in large-scale hemodynamics models via network uncertainty quantification and reduced-order modeling. Computer Methods in Applied Mechanics and Engineering, 358:112626, 2020.
- [6] Sofia Guzzetti, Simona Perotto, and Alessandro Veneziani. Hierarchical model reduction for incompressible fluids in pipes. *International Journal for Numerical Methods in Engineering*, 114(5):469–500, 2018.
- [7] Adrien Lefieux, Sara Bridio, David Molony, Marina Piccinelli, Claudio Chiastra, Habib Samady, Francesco Migliavacca, and Alessandro Veneziani. Semi-automatic reconstruction of patient-specific stented coronaries based on data assimilation and computer aided design. Cardiovascular Engineering and Technology, pages 1–18, 2022.
- [8] Claire Yilin Lin, Alessandro Veneziani, and Lars Ruthotto. Numerical methods for polyline-to-point-cloud registration with applications to patient-specific stent reconstruction. International Journal for Numerical Methods in Biomedical Engineering, 34(3):e2934, 2018.
- [9] Tiziano Passerini, Laura M Sangalli, Simone Vantini, Marina Piccinelli, Susanna Baci-galuppi, Luca Antiga, Edoardo Boccardi, Piercesare Secchi, and Alessandro Veneziani. An integrated statistical investigation of internal carotid arteries of patients affected by cerebral aneurysms. Cardiovascular Engineering and Technology, 3(1):26-40, 2012.
- [10] Maria Restrepo, Mark Luffel, Jake Sebring, Kirk Kanter, Pedro Del Nido, Alessandro Veneziani, Jarek Rossignac, and Ajit Yoganathan. Surgical planning of the total cavopulmonary connection: robustness analysis. *Annals of biomedical engineering*, 43(6):1321–1334, 2015.
- [11] Huijuan Xu. Efficient modeling of incompressible flows with moderate large Reynolds numbers using a deconvolution-based Leray model: analysis, uncertainty quantification and application in aortic dissections. PhD thesis, Georgia Institute of Technology, 2020.
- [12] Huijuan Xu, Davide Baroli, and Alessandro Veneziani. Global sensitivity analysis for patient-specific aortic simulations: The role of geometry, boundary condition and large eddy simulation modeling parameters. *Journal of Biomechanical Engineering*, 143(2), 2021.

[13] Huijuan Xu, Marina Piccinelli, Bradley G Leshnower, Adrien Lefieux, W Robert Taylor, and Alessandro Veneziani. Coupled morphological-hemodynamic computational analysis of type b aortic dissection: a longitudinal study. *Annals of biomedical engineering*, 46(7):927–939, 2018.

Numerical methods for fluid - elastic/poroelastic structure interaction problems with biomedical applications

Martina Bukač

(joint work with Catalin Trenchea)

Fluid-structure interaction (FSI) problems arise in many applications, and are characterized by highly non-linear nature. In FSI problems where the dynamics are not known, or in which the variables are changing rapidly, the robust, adaptive time-stepping is central to accurately and efficiently predict the long-term behavior of the solution. Hence, we first focus on discussing the development of a partitioned, adaptive time-stepping method for FSI problems. The proposed numerical scheme is based on the refactorized Cauchy's one-legged 'theta-like' method, which consists of a backward Euler method, where the fluid and structure sub-problems are sub-iterated until convergence, followed by a forward Euler method. The bulk of the computation is done by the backward Euler method, as the forward Euler step is equivalent to (and implemented as) a linear extrapolation. After the solution is computed, the time step, τ , is adapted based on the following formula:

$$\tau^{new} = \tau^n s \left(\frac{\delta}{\|\widehat{T}^{n+1}\|} \right)^{\frac{1}{3}},$$

where \widehat{T}^{n+1} is the local truncation error at time t^{n+1} , δ is the tolerance, and $s \in [\frac{1}{2}, 1)$ is a 'safety' parameter, routinely used to reduce the number of rejected time steps in the adaptive algorithm. The outline of the algorithm applied to a non-linear, moving domain FSI problem is given in Figure 1. The algorithm in a

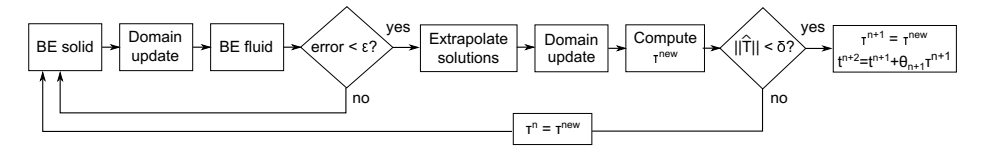


FIGURE 1. An outline of a partitioned, adaptive time-stepping numerical method for FSI problems.

fixed time-stepping version has been published in [1].

To compute the local truncation error, we use an explicit approximation to the solution calculated using a modified version of Adams-Bashforth two-step method, in which case the local truncation error is defined as

$$\widehat{T}^{n+1} = (y^{n+1} - y_{AB2}^{n+1}) \frac{1}{1 - 1/(24\mathcal{R}^n)},$$

where y^{n+1} is the solution obtained using our algorithm, y_{AB2}^{n+1} is the solution obtained using the Adams-Bashforth two-step method, and \mathbb{R}^n is given as

$$\mathcal{R}^{n} = \frac{1}{24} + \frac{1}{8} \left(1 + \frac{\tau_{n-1}}{\tau_n} \right) \left(1 + 2 \frac{\tau_{n-1}}{\tau_n} + \frac{\tau_{n-2}}{\tau_n} \right).$$

Using the formula above calculated based on the structure displacement, we obtain promising numerical results. For example, in a simulation of the blood flow in an idealized geometry, our results indicate that the smaller time step is used in systole, when the inflow velocity sharply increases, but a much larger time step can be used in diastole, helping to reduce the computational cost. Open problems related to this project involve the extension of the method to include asynchronous time stepping, and applications to more realistic problems.

The second part of this report focuses on the analysis of a diffuse interface method for the Stokes-Darcy coupled problem. In particular, we consider the interaction between a free flowing fluid and a porous medium flow, where the free flowing fluid is described using the time dependent Stokes equations, and the porous medium flow is described using Darcy's law in the primal formulation. To solve this problem numerically, we use the diffuse interface approach, where the weak form of the coupled problem is written on an extended domain which contains both Stokes and Darcy regions. This is achieved using a phase-field function, Φ , which equals one in the Stokes region and zero in the Darcy region, and smoothly transitions between these two values on a diffuse region of width ϵ around the Stokes-Darcy interface. The phase-field function is regularized as:

$$\Phi^{\epsilon} = (1 - 2\delta)\Phi^{\epsilon} + \delta.$$

where δ is a small positive number.

Our work focuses on the analysis of convergence of the diffuse interface formulation to the sharp interface formulation. This is performed by analyzing the modeling error of the diffuse interface approach at the continuous level, and by deriving the a priori error estimates for the diffuse interface method at the discrete level. To analyze the modeling error, we let $\epsilon, \delta \to 0$, and obtain $\mathcal{O}(\epsilon^{\frac{1}{2}})$. The convergence analysis of the finite element approximation of the diffuse interface method gives the convergence rates which involve terms multiplied by δ^{-1} and δ^{-2} . However, our numerical results show optimal rates of convergence that do not depend on δ . An open question related to this work is: Could the analytical results be improved?

References

[1] Martina Bukač, Anyastassia Seboldt, and Catalin Trenchea. Refactorization of cauchy's method: A second-order partitioned method for fluid—thick structure interaction problems. Journal of Mathematical Fluid Mechanics, 23(3):1–25, 2021.

Additive Manufacturing. A world full of opportunities and challenges!

FERDINANDO AURICCHIO

(joint work with coauthors)

Additive Manufacturing (AM) - also known as 3D printing - is taking off in many industrial processes. In particular, powder bed fusion for metal manufacturing has definitively changed the way of prototyping metal parts but also plastic 3D printing is changing modern engineering in many aspects. However, AM is a complex physical process, involving different thermo-mechanical phenomena at very different scales; accordingly, simulation is fundamental to predict temperature and stress distributions during and after the printing process. Furthermore, AM allows for new unknown freedom in terms of complex shapes which can be manufactured, opening the door to a new set of design requirements.

After a short introduction to the technology and possible applications, the presentation has focused on open problems of interest for the audience community and in particular on the following problems:

- structural optimization problem allowing the possibility of distributing material with different density in a specific design domain
- optimal deposition path for fiber-oriented technologies
- immersed two-level methods (in space and time) to describe highly non-linear local problems

Some advances in isogeometric analysis of coupled and complex problems

Alessandro Reali

(joint work with Alessia Patton)

Isogeometric Analysis (IGA) is a successful simulation framework originally proposed by T.J.R. Hughes and coworkers in 2005 [1] with the aim of bridging Computational Mechanics and Computer Aided Design. In addition to this, thanks to the high-regularity properties of its basis functions, IGA has shown a better accuracy per degree-of-freedom and an enhanced robustness with respect to standard finite elements in many applications - ranging from solids and structures to fluids, as well as to different kinds of coupled problems - opening also the door for the approximation in primal form of higher-order partial differential equations [2].

After a concise introduction of the basic isogeometric concepts, this lecture aims at presenting an overview of some recent advances in IGA with a special focus on coupled problems, where the characteristics of IGA seem to be of great advantage. In particular, applications that will be discussed include the simulation of fluid-structure interaction in different contexts like, e.g., biomechanical problems [3], studies on the effect of mechanically-induced stresses on prostate cancer growth [4], electro-mechanical simulations for biological tissues [5], and the use of phase-field modeling for fracture [6] or for predicting the polarization evolution in elastic ferroelectric materials [7]. The last part of the presentation will be finally devoted

to the description of a simple, accurate, and inexpensive simulation technique for laminated structures, allowed by the peculiar IGA features. In particular, this approach, originally proposed in [8], takes advantage of the favorable properties of IGA discretizations to efficiently simulate the behavior of laminated structures comprising a large number of layers using only a single element through the thickness and a post-processing technique able to recover an accurate out-of-plane stress state by direct integration of the equilibrium equations in strong form. The idea has also been successfully applied to isogeometric collocation in [9]. The convincing results of the extension of this approach to the cases of curved structures [10] and of Kirchhoff plates [11], even in an immersed framework [12], are finally shown, as well.

- T.J.R. Hughes, J.A. Cottrell, Y. Bazilevs. Isogeometric analysis: CAD, finite elements, NURBS, exact geometry and mesh refinement. Comp. Meth. Appl. Mech. Eng., 194 (2005), 4135–4195.
- [2] J.A. Cottrell, T.J.R. Hughes, Y. Bazilevs. Isogeometric Analysis: Toward integration of CAD and FEA. Wiley, 2009.
- [3] F. Xu, S. Morganti, R. Zakerzadeh, D. Kamensky, F. Auricchio, A. Reali, T.J.R. Hughes, M.S. Sacks, M.-C. Hsu. A framework for designing patient-specific bioprosthetic heart valves using immersogeometric fluid-structure interaction analysis. Int. J. Num. Meth. Biom. Eng., 34 (2018), e2938.
- [4] G. Lorenzo, T.J.R. Hughes, P. Dominguez-Frojan, A. Reali, H. Gomez. Computer simulations suggest that prostate enlargement due to benign prostatic hyperplasia mechanically impedes prostate cancer growth. Proc. Nat. Acad. Sci. of the U.S.A., 116 (2019), 1152–1161.
- [5] A. Nitti, J. Kiendl, A. Gizzi, A. Reali, M.D. de Tullio. A curvilinear isogeometric framework for the electromechanical activation of thin muscular tissues. Comp. Meth. Appl. Mech. Eng., 382 (2021), 113877.
- [6] A. Marengo, A. Patton, M. Negri, U. Perego, A. Reali. Phase-field modeling for polarization evolution in ferroelectric materials via an isogeometric collocation method. Comp. Meth. Appl. Mech. Eng., 387 (2021), 114137.
- [7] P. Fedeli, A. Frangi, F. Auricchio, A. Reali. Phase-field modeling for polarization evolution in ferroelectric materials via an isogeometric collocation method. Comp. Meth. Appl. Mech. Eng., 351 (2019), 789–807.
- [8] J.-E. Dufour, P. Antolin, G. Sangalli, F. Auricchio, A. Reali. A cost-effective isogeometric approach for composite plates based on a stress recovery procedure. Compos. Part B, 138 (2018), 12–18.
- [9] A. Patton, J.-E. Dufour, P. Antolin, A. Reali. Fast and accurate elastic analysis of laminated composite plates via isogeometric collocation and an equilibrium-based stress recovery approach. Comp. Struct., 225 (2019), 111026.
- [10] A. Patton, P. Antolin, J. Kiendl, A. Reali. Efficient equilibrium-based stress recovery for isogeometric laminated curved structures. Comp. Struct., 272 (2021), 113975.
- [11] A. Patton, P. Antolin, J.-E. Dufour, J. Kiendl, A. Reali. Accurate equilibrium-based interlaminar stress recovery for isogeometric laminated composite Kirchhoff plates. Comp. Struct., 256 (2021), 112976.
- [12] A. Patton, M. Carraturo, F. Auricchio, A. Reali. Cost-effective and accurate interlaminar stress modeling of composite Kirchhoff plates via immersed isogeometric analysis and equilibrium. J. Mech., in press (2022), https://doi.org/10.1093/jom/ufac005.

Mixed formulations for poroelasticity/free-flow using total pressure RICARDO RUIZ-BAIER

(joint work with Wietse M. Boon, Martin Hørnkjol, Miroslav Kuchta, Kent-André Mardal, Matteo Taffetani, Hans D. Westermeyer, Ivan Yotov)

We consider a multiphysics model for the flow of Newtonian fluid coupled with Biot consolidation equations through an interface Σ (see, e.g., [3]). Let $t \in (0, t_{\text{end}}]$ and take a bounded connected Lipschitz spatial domain $\Omega \subset \mathbb{R}^d$, d = 2, 3:

$$-\operatorname{div}[2\mu_{f}\boldsymbol{\epsilon}(\boldsymbol{u}) - p_{F}\mathbf{I}] = \rho_{f}\boldsymbol{g}; \quad \operatorname{div}\boldsymbol{u} = 0 \quad \text{in } \Omega_{F} \times (0, t_{\text{end}}],$$

$$(1) \quad -\operatorname{div}[2\mu_{s}\boldsymbol{\epsilon}(\boldsymbol{d}) - \varphi\mathbf{I}] = \rho_{s}\boldsymbol{f}; \quad \varphi - \alpha p_{P} + \lambda \operatorname{div}\boldsymbol{d} = 0 \quad \text{in } \Omega_{P} \times (0, t_{\text{end}}],$$

$$(C_{0} + \frac{\alpha^{2}}{\lambda})\frac{1}{\Delta t}p_{P} - \frac{\alpha}{(\Delta t)\lambda}\varphi - \operatorname{div}\left(\frac{\kappa}{\mu_{f}}\nabla p_{P} - \rho_{f}\boldsymbol{g}\right) = m_{P} \quad \text{in } \Omega_{P} \times (0, t_{\text{end}}].$$

We consider mixed boundary conditions on both subdomains and the transmission conditions on Σ are (where T_n , T_t denote normal and tangential trace operators)

$$T_{n}\boldsymbol{u} = T_{n}(\frac{1}{\Delta t}\boldsymbol{d} - \frac{\kappa}{\mu_{f}}\nabla p_{P}); \quad T_{n}(2\mu_{f}\boldsymbol{\epsilon}(\boldsymbol{u}) - p_{F}\mathbf{I}) = T_{n}(2\mu_{s}\boldsymbol{\epsilon}(\boldsymbol{d}) - \varphi\mathbf{I}),$$
$$-T_{n}T_{n}(2\mu_{f}\boldsymbol{\epsilon}(\boldsymbol{u}) - p_{F}\mathbf{I}) = p_{P}; \quad -T_{n}T_{t}(2\mu_{f}\boldsymbol{\epsilon}(\boldsymbol{u}) - p_{F}\mathbf{I}) = \frac{\gamma\mu_{f}}{\sqrt{\kappa}}T_{t}(\boldsymbol{u} - \frac{1}{\Delta t}\boldsymbol{d}).$$

The stability and well-posedness of the semi-discrete problem are derived, and we also obtain the following result (see [5]).

Theorem 1. For each $\mathbf{f} \in H^1(0, t_{\text{end}}; \mathbf{L}^2(\Omega_P))$ and $p_{P,0} \in H^1_{\star}(\Omega_p)$, there exist initial data $\mathbf{u}_0 \in \mathbf{H}^1_{\star}(\Omega_F)$, $p_{F,0} \in L^2(\Omega_F)$, $\mathbf{d}_0 \in \mathbf{H}^1_{\star}(\Omega_P)$, and $\varphi_0 \in L^2(\Omega_P)$ such that the weak formulation of (1) complemented with the initial conditions $p_P(0) = p_{P,0}$, $\mathbf{d}(0) = \mathbf{d}_0$, and $\varphi(0) = \varphi_0$, has a unique solution.

A new mixed-primal finite element scheme is proposed solving for the pairs fluid velocity - pressure and displacement - total poroelastic pressure using Stokes-stable elements. Optimal convergence rates are established, which are robust with respect to λ (see Figure 1). Upon time-discretisation, we are left with the Biot-Stokes equations written in the operator form $\mathcal{A}(\boldsymbol{u},\boldsymbol{d},p_F,\varphi,p_P)^{t}=\mathcal{F}$, where

$$(2) \begin{pmatrix} -2\mu_{f} \operatorname{div} \epsilon + \frac{\gamma \mu_{f}}{\sqrt{\kappa}} T_{t}' T_{t} & -\frac{\gamma \mu_{f}}{\sqrt{\kappa}} T_{t}' & \nabla & T_{n}' \\ -\frac{\gamma \mu_{f}}{\sqrt{\kappa}} T_{t} & -2\mu_{s} \operatorname{div} \epsilon + \frac{\gamma \mu_{f}}{\sqrt{\kappa}} T_{t}' T_{t} & \nabla & -T_{n}' \\ -\operatorname{div} & -\operatorname{div} & -\frac{1}{\lambda} I & \frac{\alpha}{\lambda} I \\ T_{n} & -T_{n} & \frac{\alpha}{\lambda} I - \left(C_{0} + \frac{\alpha^{2}}{\lambda}\right) I + \frac{\kappa}{\mu_{f}} \Delta \end{pmatrix}.$$

A main challenge for these equations is the construction of solvers that scale properly for nearly incompressible solids where λ tends to infinity, as well as in the case of nearly incompressible fluids, for which C_0 approaches zero, or the nearly impermeable regime where κ is very small. These scenarios entail not only a complication at the practical and implementation level, but also a difficulty inherent to the functional setting of the abstract formulation [4].

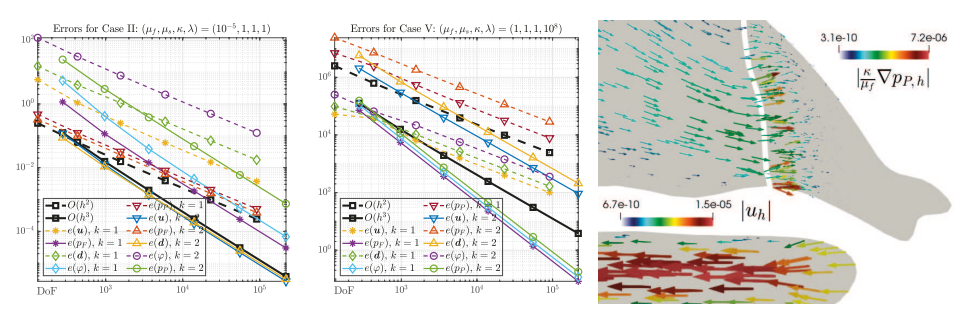


FIGURE 1. Interfacial flow in the eye, between trabecular meshwork and anterior chamber. Experimental error history and sample of axisymmetric numerical solution.

The problem defined by (2) can be shown to be well-posed using the usual space \boldsymbol{H} and its natural metric (for instance, following the analysis performed in Theorem 1). Alternatively, consider the weighted product space $\boldsymbol{H}_{\epsilon}$, where ϵ encodes the weighting parameters κ , α , γ , μ_f , μ_s , C_0 , λ . Let us group the variables as $\vec{\boldsymbol{u}} = (\boldsymbol{u}, \boldsymbol{d})$ and $\vec{p} = (p_F, \varphi, p_P)$ and introduce the weighted norm

$$\|(\vec{\boldsymbol{u}}, \vec{p})\|_{\mathbf{H}_{\epsilon}}^{2} := 2\mu_{f} \|\boldsymbol{\epsilon}(\boldsymbol{u})\|_{0,\Omega_{F}}^{2} + \frac{\gamma \mu_{f}}{\sqrt{\kappa}} \|T_{t}(\boldsymbol{u} - \boldsymbol{d})\|_{0,\Sigma}^{2} + 2\mu_{s} \|\boldsymbol{\epsilon}(\boldsymbol{d})\|_{0,\Omega_{P}}^{2}$$

$$+ \frac{1}{2\mu_{f}} \|p_{F}\|_{0,\Omega_{F}}^{2} + \frac{1}{2\mu_{s}} \|\varphi\|_{0,\Omega_{P}}^{2} + \left(\frac{1}{2\mu_{f}} + \frac{1}{2\mu_{s}}\right) \|p_{P}|_{\Sigma}\|_{-\frac{1}{2},01,\Sigma}^{2}$$

$$+ \frac{1}{\lambda} \|\varphi - \alpha p_{P}\|_{0,\Omega_{P}}^{2} + C_{0} \|p_{P}\|_{0,\Omega_{P}}^{2} + \frac{\kappa}{\mu_{f}} \|\nabla p_{P}\|_{0,\Omega_{P}}^{2},$$

which hinges on a fractional norm of the restriction of the Biot pressure to Σ . The space \mathbf{H}_{ϵ} is such that contains all (\vec{u}, \vec{p}) that are bounded in this norm (see [1]).

Theorem 2. The problem defined by the solution operator (2) is well-posed in the space \mathbf{H}_{ϵ} equipped with the norm (3).

A natural block-diagonal preconditioner for the Biot-Stokes problem is therefore the Riesz map with respect to the inner product in \mathbf{H}_{ϵ}

(4)
$$\mathcal{R} = \begin{pmatrix} \mathcal{A}_{FF} & \mathcal{A}_{FP} \\ \mathcal{A}_{PF} & \mathcal{A}_{PP} \\ \vdots & \vdots \\ \frac{1}{2\mu_f} I \\ \vdots & (\frac{1}{\lambda} + \frac{1}{2\mu_s}) I & -\frac{\alpha}{\lambda} I \\ \vdots & -\frac{\alpha}{\lambda} I & (C_0 + \frac{\alpha^2}{\lambda}) I - \frac{\kappa}{\mu_f} \Delta + \frac{1}{\mu} (-\Delta_{\Sigma,01})^{-\frac{1}{2}} \end{pmatrix}^{-1} ,$$

where $\mu^{-1} := (2\mu_s)^{-1} + (2\mu_f)^{-1}$. This preconditioner yields robustness with respect to a wide range of material parameters, as reported in Figure 2.

Several open problems and challenges arise as an extension to the results in [1, 5]. For example, the efficient realisation of the preconditioners using algebraic

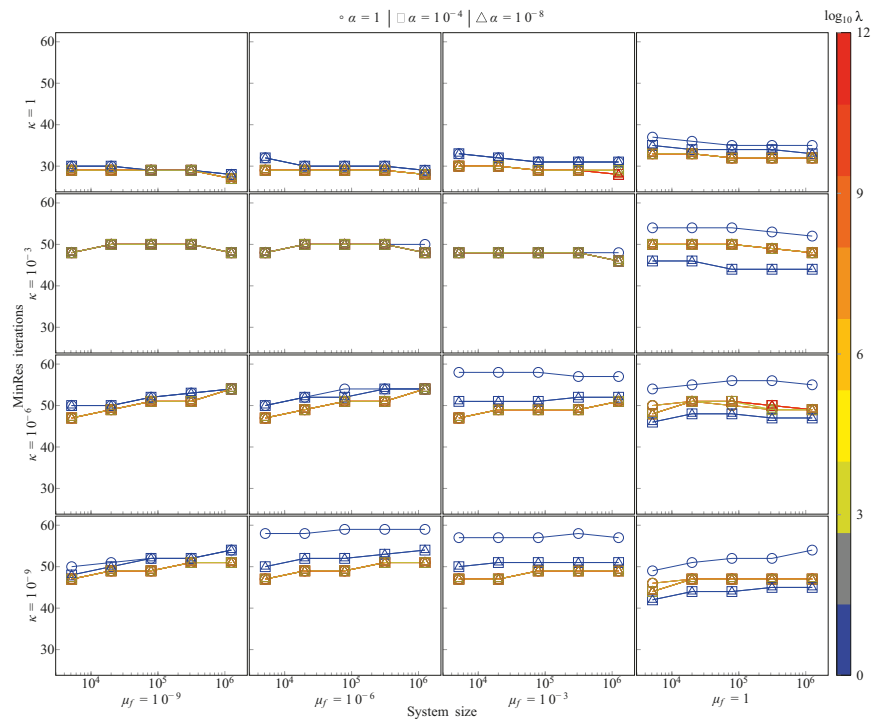


FIGURE 2. Performance of the Biot-Stokes preconditioner (4) setting μ_s , γ to 1 and $C_0 = 0$ and using TH₁ elements.

or geometric multigrid, setting up appropriate scalable solvers that maintain robustness with respect to the timestep, extending the current analysis of robust preconditioners to formulations based on four-field Biot equations (including both total pressure and Darcy flux), and generalising the model to the regime of large deformations and the incorporation of remodelling mechanisms better describing the consolidation of the interface and choking phenomena in eye poromechanics.

- [1] W. Boon, M. Hørnkjol, M. Kuchta, K.-A. Mardal, and R. Ruiz-Baier, *Parameter-robust methods for the Biot-Stokes interfacial coupling without Lagrange multipliers*, arXiv preprint http://arxiv.org/abs/2111.05653 (2021).
- [2] D. Braess, Stability of saddle point problems with penalty, ESAIM: Mathematical Modelling and Numerical Analysis 30 (1996), 731–742.
- [3] A. Cesmelioglu and P. Chidyagwai, Numerical analysis of the coupling of free fluid with a poroelastic material, Numerical Methods for PDEs 36 (2020), 463–494.
- [4] K. E. Holter, M. Kuchta, and K.-A. Mardal, Robust preconditioning for coupled Stokes— Darcy problems with the Darcy problem in primal form, Computers & Mathematics with Applications 91 (2021), 56–66.
- [5] R. Ruiz-Baier, M. Taffetani, H. D. Westermeyer, and I. Yotov, The Biot-Stokes coupling using total pressure: formulation, analysis and application to interfacial flow in the eye, Computer Methods in Applied Mechanics and Engineering 389 (2022), e114384.

A geometric approach to modeling, analysis, and numerics for fractured porous materials

Jan Martin Nordbotten

(joint work with Wietse M. Boon, Jon Eivind Vatne)

Fractures appear in many natural and engineered porous materials. Of particular interest for the current talk relates to fluid flow through the porous media and its fractures, and in particular, the case where the fractures are modeled as lower-dimensional manifolds.

Our central argument is that this problem should not be considered from the perspective of a normal continuum model, which has been perturbed by the presence of fractures. In contrast, one should consider the model as inherently mixed-dimensional, that is to say that the model equations are formulated on a collection of domains of differing topological dimension.

In the main part of the talk, we review the representation of mixed-dimensional geometries, emphasizing the role of boundary domains as hosts for coupling variables. Having established the geometric structure, we propose two generalizations of the 3D de Rham complex (gradient, curl and divergence operators). These two generalizations are not independent, indeed, they are seen to be adjoints with respect to the natural L^2 inner products for the mixed-dimensional geometry.

This foundation allows us to establish that L^2 -spaces on mixed-dimensional geometries, together with the above-mentioned differential operators, form Hilbert complexes, with the same cohomology structure as the underlying (standard) de Rham complex. This ensures that mixed-dimensional Hodge Laplace problems are well-posed in a weak sense.

Returning to the original application of modeling flow in fractured porous media, we identify that the standard models with lower-dimensional representations of fracture correspond to the "right-most" Hodge Laplacian in the de Rham complex. Consequently, well-posedness theory for the model equations for fractured porous media, in the presense of complex networks of intersecting fractures, is a corollary of this work.

From the perspective of numerical approximations, we identify that the mixed finite element subspaces can also be locally applied to form conforming subcomplex of the mixed-dimensional Hilbert complex. This directly leads to the observation that conforming mixed-finite element approximations for this problem are stable and convergent. The talk concludes with a posteriori error bounds and numerical examples. Further details can be found in the references.

REFERENCES

- Boon, W. M. and J. M. Nordbotten, Mixed-dimensional poromechanical models of fractured porous media, preprint. https://arxiv.org/abs/2112.05038
- [2] Boon, W. M., J. M. Nordbotten, J. E. Vatne, Functional analysis and exterior calculus on mixed-dimensional geometries, Ann. Mat. Pura Appl., 200(2) (2021), 757-789.
- [3] Boon, W. M., J. M. Nordbotten, I. Yotov, Robust discretization of flow in fractured porous media, SIAM J. Numer. Anal., 56(4) (2018), 2203-2233.

[4] Varela, J. E. Ahmed, E. Keilegavlen, J. M. Nordbotten, F. A. Radu, A posteriori error estimates for hierarchical mixed-dimensional elliptic equations, preprint. https://arxiv.org/abs/2101.08331

Multiscale modelling of maple sap flow

JOHN M. STOCKIE

Sap exudation is the process whereby sugar maple trees (and a few other related species) are able to generate a large positive stem pressure during winter when the tree is leafless and largely dormant. Exudation pressure is vital for the maple syrup industry since it is what allows sap to be harvested from tap-holes in large quantities before it is processed into syrup. The underlying bio-physical causes of sap exudation have been a subject of intense debate within the biological literature for over a century [2, 5]. Experiments clearly show that maple stem pressure builds up in response to repeated cycles of freeze/thaw when daily temperatures oscillate around the freezing point. Milburn and O'Malley [5] were the first to propose a physically consistent explanation for this phenomenon that takes into account distinctive features of the cellular microstructure of maple sapwood and treats the sap as a two-phase (gas-liquid) mixture whose dynamics are governed by the combined effects of heat transport, phase change, and osmotic flow through selectively-permeable cell membranes. Until recently this picture remained the definitive description for exudation, despite the increasing evidence from experiments suggesting that certain vital processes might still be missing [6].

We review the results from a series of papers [1, 3, 4] that develop the first mathematical model for the Milburn-O'Malley freeze/thaw process and incorporates the following additional physical effects:

- dissolution/nucleation of gas bubbles that are suspended within the sap,
- cryostatic suction due to the presence of ice-water interfacial tension that arises from liquid freezing within microscopic capillaries,
- root water uptake from the soil.
- freezing point depression due to the presence of sugar dissolved in the sap.

The microscale model describing these processes consists of a coupled nonlinear system of differential-algebraic equations (DAEs) that are defined on a "reference cell" Y, representing a simplified cell geometry (see Figure 1a). The freeze/thaw state is determined by 6 possible configurations of gas, liquid and ice phase interfaces within the reference cell so that there are actually 6 possible choices for DAEs to impose at a given stem location, depending on the local value of temperature.

The freeze/thaw process is driven by changes in ambient temperature occurring in the tree stem, which introduces a clear separation in spatial scales between cellular processes occurring on the microscale and heat transport on the macroscale. By tiling the tree stem with a periodic array of scaled copies εY of the reference cell (see Figure 1b) we can apply the method of periodic homogenization [4] to

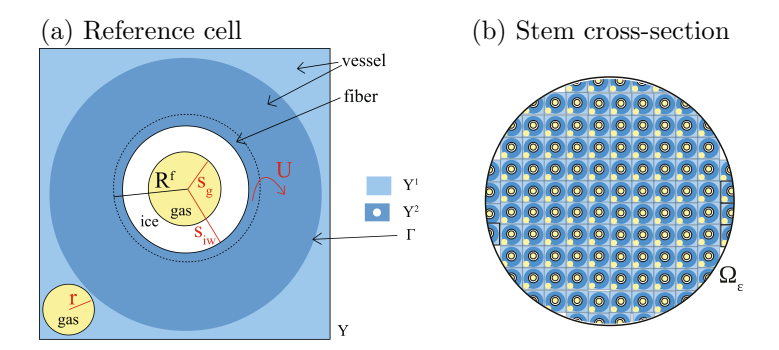


FIGURE 1. Illustration of the periodic homogenization process with: (a) reference cell Y; and (b) stem Ω_{ε} tiled with scaled copies of the reference cell, εY .

obtain an "up-scaled" heat equation in the two-scale limit as $\varepsilon \to 0$:

(1)
$$\partial_t E_1 - \nabla_x \cdot \left(\Pi D(E_1) \nabla_x T_1 \right) = \frac{1}{|Y^1|} \int_{\Gamma} D(E_2) \nabla_y T_2 \cdot \vec{n} \, dS.$$

Here, $T_1(x,t)$ and $E_1(x,t)$ are the macroscopic temperature and enthalpy defined on the stem region $x \in \Omega$, while $T_2(x,y,t)$ and $E_2(x,y,t)$ are the corresponding microscopic quantities that also depend on the location within the reference cell $y \in Y$. The homogenization procedure gives rise to two sources of coupling between the micro- and macroscale problems:

- The matrix Π multiplying the macroscopic diffusion coefficient is a geometric scaling factor that comes from solving a standard elliptic problem on the reference cell.
- The integral source term represents the contribution to the macroscale temperature owing to the latent heat of phase change. This contribution is evaluated as the heat flux across a curve Γ that bounds a liquid-filled subregion of the reference cell, $Y^1 \subset Y$ lying outside Γ (see Figure 1a).

Note that formulating the heat equation in this temperature-enthalpy form, along with a suitable definition for the thermal diffusivity function D(E), allows us to capture the liquid/solid phase interfaces naturally along with the corresponding release of latent heat. A detailed description of the two-scale model equations and their derivation can be found in [3].

The equations described above are discretized in space with a simple finite volume approach, and then integrated in time using the stiff ODE solver ode15s implemented in Matlab. Numerical comparisons are then made with temperature and pressure data obtained from red and sugar maple trees located at the University of Vermont's Proctor Maple Research Center [7]. A sample comparison for a red maple tree is plotted in Figure 2, which shows that locations of spikes (or drops) in the simulated stem pressure correlate closely with thaw (or freeze) events, which are the zero-crossings in the temperature plot. The peak value of

pressure for many of the thaw-induced spikes is also matched quite closely by the simulations, as is the rate of the pressure decay following a spike. There are some "weak" freeze/thaw events that are not captured by the simulations, but otherwise these results suggest that the sap exudation model does a reasonable job of capturing the essential physics underlying the pressure generation process in maple trees.

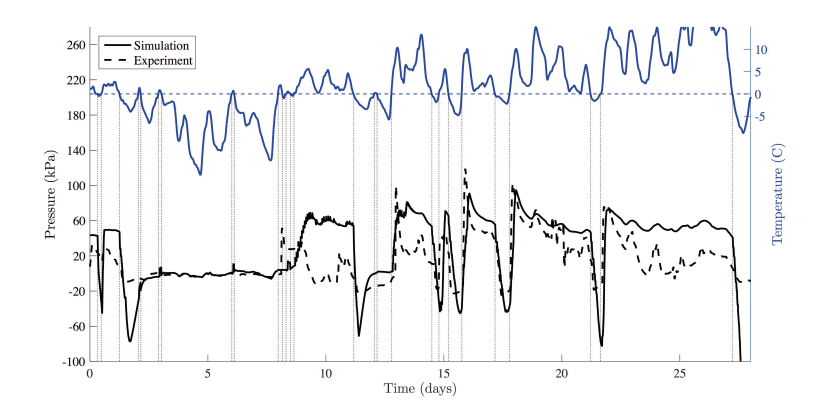


FIGURE 2. Comparison between experiments and numerical simulations for a red maple tree, showing the ambient temperature (solid blue line) and stem pressure (black dashed) measured in experiments, along with the simulated pressure (black solid). Freeze and thaw events are highlighted with dotted vertical lines.

- M. Ceseri and J. M. Stockie. A mathematical model for sap exudation in maple trees governed by ice melting, gas dissolution and osmosis. SIAM Journal on Applied Mathematics 73 (2013), 649–676.
- [2] D. Cirelli, R. Jagels, and M. T. Tyree. Toward an improved model of maple sap exudation: the location and role of osmotic barriers in sugar maple, butternut and white birch. Tree Physiology 28 (2008), 1145–1155.
- [3] I. Graf, M. Ceseri, and J. M. Stockie. Multiscale model of a freeze—thaw process for tree sap exudation. *Journal of the Royal Society Interface* 12 (2015), 20150665.
- [4] I. Konrad, M. A. Peter, and J. M. Stockie. A two-scale Stefan problem arising in a model for tree sap exudation. IMA Journal of Applied Mathematics 82 (2017), 726–762.
- [5] J. A. Milburn and P. E. R. O'Malley. Freeze-induced sap absorption in Acer pseudoplatanus: a possible mechanism. Canadian Journal of Botany 62 (1984), 2101–2106.
- [6] M. T. Tyree. The mechanism of maple sap exudation. In Terazawa et al. (eds.), Tree Sap: Proceedings of the First International Symposium on Sap Utilization, Bifuka, Japan (1995), 37–45.
- [7] M. Zarrinderakht, I. Konrad, A. van den Berg, T. R. Wilmot, T. D. Perkins, and J. M. Stockie. Experimental and computational comparison of freeze—thaw induced pressure generation in red and sugar maple. *Tree Physiology* (2022), under revision.

Mixed-dimensional coupling of 1D geometrically exact beam finite elements and 3D continua for engineering applications

Alexander Popp

(joint work with Nora Hagmeyer, Matthias Mayr, Ivo Steinbrecher)

The interaction of rod- or beam-like structures with three-dimensional continua can be found in a variety of different physical problems ranging from classical engineering (e.g. fiber-reinforced materials of any kind) to biomedical applications (e.g. stents for endovascular interventions). Truly mixed-dimensional 1D-3D coupling along with suitable finite element discretization schemes offers a promising framework for high-fidelity numerical simulations [1, 2, 3].

Our baseline approach [1] deals with the consistent embedding of curved 1D Cosserat continua (i.e. beams) into 3D solid volumes. The beams are explicitly modeled with 1D geometrically exact beam finite elements, while the surrounding solid volume is modeled with 3D continuum (solid) elements. Arguably, the most natural choice for the coupling conditions is to couple the beam surface $\delta\Omega_B^0$ to the solid volume Ω_S^0 in the reference configuration. This approach would lead to a 2D-3D coupling formulation, i.e. the beam surface is embedded into the background solid volume. For the inherent assumption in this work, that the cross-section dimensions of the beam are small compared to the other dimensions of the coupled problem, we can approximate the surface integrals as line integrals along the beam axis. These line integrals can be evaluated very efficiently, and the physical coupling dimensionality changes from surface-to-volume coupling (2D–3D) to line-to-volume coupling (1D–3D). Exemplarily, the coupling contribution to the resulting variational formulation (i.e. coupling virtual work δW_c) becomes

(1)
$$\delta W_c^{\text{2D-3D}} \approx \delta W_c^{\text{1D-3D}} = \int_{\Gamma^{\text{1D-3D}}} \underline{\boldsymbol{\lambda}}^{\text{1D-3D}} \left(\delta \underline{\boldsymbol{u}}_r^B - \delta \underline{\boldsymbol{u}}^S \right) ds ,$$

where $\underline{\boldsymbol{\lambda}}^{\text{1D-3D}}$ is a Lagrange multiplier vector defined along the beam centerline (or a line load when interpreted physically), while $\underline{\boldsymbol{u}}_r^B$ and $\underline{\boldsymbol{u}}_r^S$ represent the unknown displacement fields of the beam centerline and solid, respectively. A mortar-type approach is employed to enforce the kinematic coupling constraints on inevitably non-matching and mixed-dimensional meshes. This discrete formulation follows closely the well-established concept of equidimensional (3D-3D) mortar finite element methods, while carefully taking into account the peculiarities of mixed-dimensional (1D-3D) coupling, e.g. for integration interval segmentation and the handling of weak and strong discontinuities within the mortar integrals. The inf-sup stability of the mixed formulation is practically assured by a simple choice of the discrete Lagrange multiplier basis $\underline{\boldsymbol{\lambda}}^{\text{1D-3D}} = \sum_j \Phi_j \boldsymbol{\lambda}_j$ through first-order Lagrange polynomials Φ_j , yet a theoretical proof is still missing.

The new approach has been verified and validated with an extensive set of benchmark examples, such as convergence studies under uniform mesh refinement, see Figure 1. Optimal convergence rates of the coupled model can only be expected up to a certain degree of mesh refinement in the solid domain. This is due to the obvious singularity introduced by the mixed-dimensional embedded coupling formulation. From a mechanical point of view, the proposed 1D-3D coupling is equivalent to a line load acting inside the solid domain. This represents a generalized version of the well-known Kelvin problem, which consists of an infinite solid domain into which a line load is embedded. Nonetheless, our numerical examples convincingly illustrate that optimal convergence behavior is indeed preserved for relevant physical application scenarios of the proposed 1D-3D approach, i.e. relatively slender and stiff fibers compared to the surrounding material.

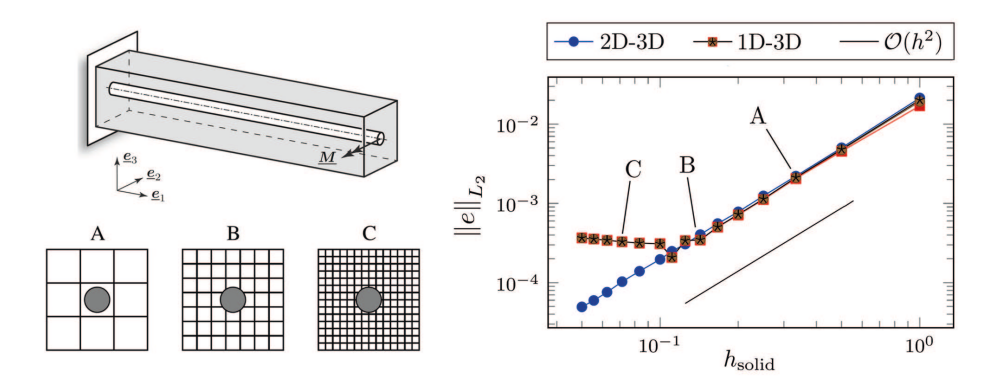


FIGURE 1. Convergence problem setup (top left), L_2 error (right) and characteristic meshes with hex8 elements (bottom left).

Recently, the baseline approach has been extended towards additional model complexities, such as the coupling of the beam's rotational degrees of freedom [2], the 1D-2D coupling of beams and solid surfaces as well as 1D-3D fluid-structure interaction [3]. Among the many open challenges discussed during the Oberwolfach workshop is a model transition in the spirit of homogenization theory in order to recover optimal convergence also in the asymptotic (mesh refinement) limit.

- I. Steinbrecher, M. Mayr, M.J. Grill, J. Kremheller, C. Meier, A. Popp, A mortar-type finite element approach for embedding 1D beams into 3D solid volumes, Computational Mechanics 66 (2020), 1377–1398.
- [2] I. Steinbrecher, A. Popp, C. Meier, Consistent coupling of positions and rotations for embedding 1D Cosserat beams into 3D solid volumes, Computational Mechanics (2021), https://doi.org/10.1007/s00466-021-02111-4.
- [3] N. Hagmeyer, M. Mayr, I. Steinbrecher, A. Popp, Fluid-beam interaction: Capturing the effect of embedded slender bodies on global fluid flow and vice versa, arXiv Preprint (2022), https://arxiv.org/abs/2104.09844.

Discontinuous Galerkin Methods for Green-Naghdi Models Coupled with Geomorphology

CLINT DAWSON

(joint work with Kazbek Kazhyken and Juha Videman)

In shallow water with highly energetic waves, the standard shallow water equations do not capture so-called "dispersive wave phenomena". In these environments, waves of different wave lengths travel with different phase speeds. Various mathematical models have been proposed over the years to capture waves of different wave lengths, ranging from Boussinesq models to full Navier-Stokes models. Green-Naghdi models of various complexities have been proposed which can approximate many different types of waves and transition easily from shallow water to dispersive wave phenomena within a single model. In recent work, we studied the numerical solution of this model using hybrid discontinuous Galerkin methods [1]. In this talk, we extend this work to include sediment transport and bed erosion (geomorphology). This gives rise to coupled, highly nonlinear, multiscale models. We discuss the implementation of the hybrid DG scheme and its applications to various laboratory experiments, which show good agreement overall. We then discuss the main motivation of this work, which is studying the Ria Formosa Lagoon on the southern coast of Portugal. This is a highly energetic wave environment where dispersive waves, and geomorphological effects, are all present. This region has extremely complex geometry, in addition to transitioning from deep ocean currents to very shallow lagoons within kilometers. We discuss how we obtained data to build a finite element model, and then show simulation results to demonstrate that the addition of dispersive wave terms gives rise to additional geomorphological effects in the entrances to the lagoons under normal tidal conditions. This work is described in [2, 3].

- [1] Samii, A. and Dawson, C., An explicit hybridized discontinuous Galerkin method for Serre-Green-Naghdi wave model, Computer Methods in Applied Mechanics and Engineering, 330 (2018), 447-470, https://doi.org/10.1016/j.cma.2017.11.001.
- [2] Kazhyken, Kazbek, Videman, Juha and Dawson, Clint, Discontinuous Galerkin methods for a dispersive wave hydro-sediment-morphodynamic model, Computer Methods in Applied Mechanics and Engineering, 377 (2021), https://doi.org/10.1016/j.cma.2020.113592.
- [3] Kazhyken, Kazbek, Videman, Juha and Dawson, Clint, Discontinuous Galerkin methods for a dispersive wave hydro-morphodynamic model with bed-load transport, Computer Methods in Applied Mechanics and Engineering, 375 (2021), https://doi.org/10.1016/j.cma.2021.113684.

Global-in-time Domain Decomposition Methods for Coupled Problems in Heterogeneous Porous Media

Thi-Thao-Phuong Hoang

Global-in-time domain decomposition (GT-DD) methods are iterative algorithms that solve time-dependent problems in the subdomains over the whole time interval and exchange data on the space-time interfaces between the subdomains. These methods can be seen as a combination of the classical waveform relaxation method for a large system of ODEs and standard DD methods for steady-state problems. GT-DD is different from the classical DD approach where the model problem is first discretized in time by an implicit scheme, then at each time step the iteration is performed and involves the solution of stationary problems in the subdomains. The same time step is usually imposed on the whole domain for classical DD methods, while for GT-DD, different time steps can be used in different regions of the domain. Thus GT-DD is very well-suited for parallel simulations of multiscale coupled problems which often require local discretizations in both space and time. It should be noted that GT-DD is fully implicit, and has no time step restriction for stability reasons as normally required in (non-iterative) partitioned time-stepping algorithms. There are basically two classes of GT-DD methods: Schur-type and Schwarz-type methods. The former is based on the physical transmission conditions while the latter is based on more general (optimized) transmission conditions such as Robin or Ventcel conditions [3, 2]. Using a substructuring technique, GT-Schur or GT-Schwarz methods can be reduced to a space-time interface problem which is solved iteratively (e.g., by GMRES) and globally in time.

In this talk, we present the development of GT-DD methods for the reduced fracture flow model and the (nonlinear) Stokes-Darcy system. We write the problems in mixed form and consider conforming meshes for spatial discretization as our focus here is local time stepping. The proposed methods can be extended to nonmatching spatial grids via mortar finite elements as recently studied in [8] for the case with no fractures. The talk is based on joint work with Yanzhao Cao, Phuoc-Toan Huynh, Caroline Japhet, Michel Kern, Hemanta Kunwar, Hyesuk Lee and Jean Roberts; more details can be found in [4, 7, 6, 5].

Global-in-time DD for the reduced fracture flow model. We consider a reduced fracture model in which the fracture is known a priori and is modeled as a hypersurface embedded in the porous medium. Let Ω be a bounded domain separated by a fracture-interface γ into two connected subdomains Ω_1 and Ω_2 . We assume that the permeability in the fracture is higher than the surrounding rock matrix, so that the pressure is continuous across the fracture [1]. We construct DD formulations by using the pressure continuity equation and tangential PDEs in the fracture-interface as transmission conditions:

(1)
$$p_i = p_{\gamma},$$
 on $\gamma \times (0, T), i = 1, 2,$

(2)
$$\phi_{\gamma} \partial_{t} p_{\gamma} + \operatorname{div}_{\tau} \boldsymbol{u}_{\gamma} = q_{\gamma} + \sum_{i=1}^{2} (\boldsymbol{u}_{i} \cdot \boldsymbol{n}_{i})_{|\gamma} \quad \text{in } \gamma \times (0, T), \\ \boldsymbol{u}_{\gamma} = -\boldsymbol{K}_{\gamma} \delta \nabla_{\tau} p_{\gamma} \quad \text{in } \gamma \times (0, T),$$

where δ is the fracture width. Inspired by the global-in-time optimized Schwarz method for the case without fractures, we introduce new transmission conditions, namely Ventcel-to-Robin conditions, by taking linear combinations (for a positive parameter α) of the physical transmission conditions (1)-(2):

(3)
$$-\mathbf{u}_{i} \cdot \mathbf{n}_{i} + \alpha p_{i,\gamma} + \phi_{\gamma} \partial_{t} p_{i,\gamma} + \operatorname{div}_{\tau} \mathbf{u}_{\gamma,i} = -\mathbf{u}_{j} \cdot \mathbf{n}_{i} + \alpha p_{j,\gamma} \\ \mathbf{u}_{\gamma,i} = -\mathbf{K}_{\gamma} \delta \nabla_{\tau} p_{i,\gamma}$$
 on $\gamma \times (0,T)$,

for i = 1, 2, and j = (3 - i). We have introduced Lagrange multipliers $p_{i,\gamma}$ representing the trace of p_i on γ , and defined $\mathbf{u}_{\gamma,i}$ as the tangential velocity in the fracture associated with the pressure p_i . Based on either (1)-(2) or (3), we proposed the following four GT-DD methods [4, 7]:

- (i) Global-in-time primal Schur (GTP-Schur): This method is based on the time-dependent Dirichlet-to-Neumann operators and its interface unknown λ represents the fracture pressure p_{γ} .
- (ii) Global-in-time dual Schur (GTD-Schur): This is the dual version of the first method, which uses the time-dependent Neumann-to-Dirichlet operators. Unlike the standard dual Schur method, two interface unknowns φ_1 and φ_2 are introduced representing $\mathbf{u}_1 \cdot \mathbf{n}_1|_{\gamma}$ and $\mathbf{u}_2 \cdot \mathbf{n}_2|_{\gamma}$, since the normal flux may not be continuous across the fracture-interface.
- (iii) Global-in-time fracture-based Schur (GTF-Schur): This is a novel method typically designed for the reduced fracture model. The interface unknown is the total flux $\varphi := \mathbf{u}_1 \cdot \mathbf{n}_1|_{\gamma} + \mathbf{u}_2 \cdot \mathbf{n}_2|_{\gamma}$, which is used to solve the flow problem in the fracture to recover p_{γ} . GTF-Schur also uses the Dirichlet-to-Neumann operators as GTP-Schur, however, a different interface problem is formulated by matching the sum of the normal fluxes from the subdomains with φ .
- (iv) Global-in-time optimized Schwarz (GTO-Schwarz): Unlike the Schur-type methods, here we consider Ventcel-to-Robin transmission conditions (instead of the physical ones). Consequently, GTO-Schwarz uses the time-dependent Ventcel-to-Robin operators and two interface unknowns are introduced representing the Ventcel term for each subdomain.

GTP-Schur and GTD-Schur need efficient preconditioners for satisfactory convergence, while GTF-Schur requires no preconditioning as its interface operator is the identity operator. The convergence of GTO-Schwarz is accelerated by optimizing the parameter α via the framework of optimized Schwarz waveform relaxation [4]. When smaller time steps are used in the fracture and larger ones in the subdomains, numerical results (for non-immersed and partially immersed fracture problems [7]) show that only the preconditioned GTD-Schur and the GTF-Schur give smaller errors in the fracture; the errors by the preconditioned GTP-Schur and the GTO-Schwarz are the same as those with conforming coarse time steps on the whole domain. Thus GTF-Schur is the most efficient method in terms of fast convergence and preserving the accuracy with nonconforming time grids.

Global-in-time DD for the Stokes-Darcy coupling. We consider the interaction between a free non-Newtonian fluid flow (governed by the nonlinear Stokes equations) in Ω_f with a porous medium flow (governed by the nonlinear Darcy

equations in mixed form) in Ω_p . On the space-time interface $\Gamma \times (0, T)$, the following transmission conditions to enforce mass conservation, balance of the normal forces and the Beavers-Joseph-Saffman law are imposed:

(4a)
$$\mathbf{u}_f \cdot \mathbf{n}_f + \mathbf{u}_p \cdot \mathbf{n}_p = 0,$$

(4b)
$$-\boldsymbol{n}_f \cdot (\nu_f(|\boldsymbol{D}(\boldsymbol{u}_f)|)\boldsymbol{D}(\boldsymbol{u}_f) - p_f \boldsymbol{I}) \cdot \boldsymbol{n}_f = p_p,$$

$$(4c) -\boldsymbol{n}_f \cdot (\nu_f(|\boldsymbol{D}(\boldsymbol{u}_f)|)\boldsymbol{D}(\boldsymbol{u}_f) - p_f \boldsymbol{I}) \cdot \boldsymbol{t}_j = c_{BJS} \boldsymbol{u}_f \cdot \boldsymbol{t}_j, \ j = 1, \dots, d-1.$$

Only equations (4a) and (4b) are coupling conditions between the free fluid flow and porous medium flow. They can be rewritten equivalently as Robin conditions (for positive parameters α_p and α_f):

(5a)
$$\boldsymbol{n}_f \cdot (p_f \mathbf{I} - \nu_f \boldsymbol{D}(\boldsymbol{u}_f)) \cdot \boldsymbol{n}_f - \alpha_f \boldsymbol{u}_f \cdot \boldsymbol{n}_f = p_p + \alpha_f \boldsymbol{u}_p \cdot \boldsymbol{n}_p$$
, on $\Gamma \times (0, T)$,

(5b)
$$p_p - \alpha_p \boldsymbol{u}_p \cdot \boldsymbol{n}_p = \boldsymbol{n}_f \cdot (p_f \mathbf{I} - \nu_f D(\boldsymbol{u}_f)) \cdot \boldsymbol{n}_f + \alpha_p \boldsymbol{u}_f \cdot \boldsymbol{n}_f$$
, on $\Gamma \times (0, T)$.

GT-DD methods can be developed based on either the physical transmission conditions (4a)-(4b) or Robin conditions (5). Advantages of such an approach are that smaller time steps in the fluid region can be coupled with larger time steps in the porous medium, and stable long-term simulations can be carried out with no restrictions on the time step sizes. In [6], a GT-Schur method was constructed for the nonlinear Stokes-Darcy system, which leads to a nonlinear space-time interface problem. A nested iteration approach was proposed: we linearize the nonlinear interface problem by Newton algorithm, then at each Newton iteration, we solve the linearized interface problem (globally in time) by GMRES. In [5], a GT-Schwarz method with Robin conditions was considered and its convergence was proved for the constant viscosity functions (i.e., linear problems) given that $\alpha_p \geq \alpha_f$. Numerical results suggest that the ratio between α_p and α_f must be sufficiently large in order to obtain expected accuracy in time.

- C. Alboin, J. Jaffre, J.E. Roberts, C. Serres, Modeling fractures as interfaces for flow and transport in porous media, Contemp. Math., Amer. Math. Soc., 295 (2002), 13–24.
- [2] D. Bennequin, M.J. Gander, L. Gouarin, L. Halpern, A homographic best approximation problem with application to optimized Schwarz waveform relaxation, Math. Comp. 78 (2009), 185–223.
- [3] M.J. Gander and L. Halpern, Optimized Schwarz waveform relaxation for advectionreaction-diffusion problems, SIAM J. Numer. Anal. 45(2007), 666-697.
- [4] T.T.P. Hoang, C. Japhet, M. Kern & J. E. Roberts, Space-time domain decomposition for reduced fracture models in mixed formulation, SIAM J. Numer. Anal., 54 (2016), 288–316.
- [5] T.T.P. Hoang, H. Kunwar & H. Lee, Nonconforming time discretization based on Robin transmission conditions for the Stokes-Darcy system, Appl. Math. Comput., 413, 2022.
- [6] T.T.P. Hoang & H. Lee, A global-in-time domain decomposition method for the coupled nonlinear Stokes and Darcy flows, J. Sci. Comput., 87, 2021.
- [7] P.T. Huynh, Y.Cao & T.T.P. Hoang, Fast and accurate domain decomposition methods for reduced fracture models with nonconforming time grids, Preprint, 2022, arxiv.org/abs/2202.06116
- [8] M. Jayadharan, M. Kern, M. Vohralík & I. Yotov, A space-time multiscale mortar mixed finite element method for parabolic equations, Preprint, 2021, arxiv.org/abs/2110.02132.

Agent–based and continuum–based mechanics in medical processes

Fred Vermolen

(joint work with Qiyao Peng, Ginger Egberts, Wietse Boon)

In order to optimise therapies applied to various diseases, it is necessary to understand the underlying biophysical mechanisms that are occurring in the body. To validate the developed theoretical framework against clinical observations and in-vitro experiments, the framework is translated into quantitative relations that build up a mathematical framework. The mathematical frameworks consist of (combinations of) algebraic equations, (partial) differential equations and stochastic processes. Here, we deal with mathematical model frameworks for the evolution of skin after burn injuries and the evolution of growth of tumors and the possible subsequent metastasis of cancer. However, the focus of the current abstract lies on burn injuries.

Severe burn injuries and other types of deep tissue injury are characterised by damage on multiple layers of skin, such as the epidermis, dermis and possibly even the subcutis. The epidermis consists of epithelial cells (keratinocytes) and usually heals without any complications. The biological mechanism behind healing is cell division (proliferation) and cell migration by cellular contact forces and random walk (diffusion). This mode of healing is commonly referred to as wound closure. Once the epithelial layer has been restored, then practitioners usually no longer speak of a wound, but of a scar if the layers underneath have been damaged. Since the dermal layer consists of collagen (which is the extracellular matrix that supports the integrity of skin) and of small blood vessels and several cell types such as, among others, fibroblasts and endothelial cells, the evolution of this layer of skin is very different from the epidermal layer.

The evolution of the scar proceeds by a chain of biophysical processes, which involve the coagulation of blood, build up of a provisional fibrin network (hemostasis), the clearing up of contaminants and pathogens by immune cells (inflammatory response), replacement of fibrin network by regenerated collagen and regeneration of a network of small blood vessels (proliferative phase) and finally the reinforcement of the collagen structure (remodelling). The presentation mainly covered the proliferative phase where fibroblasts migrate into the wound area, and where they secrete collagen. From an evolutionary point of view, it is advantageous in case of deep tissue injury that the wound area reduces in order to minimise the influx of contaminants and pathogens. However, in a burn injury, this reduction of area is not favourable. Nevertheless, this undesirable reduction of area, referred to as contraction, often takes place in deep burn injuries. This is caused by the differentiation of fibroblasts into myofibroblasts, which exert large pulling forces on their direct environment. Severe contractions may cause dysfunctioning of joints and limbs and, in some extreme cases, even disability of patients.

The full mathematical frameworks that describes the interplay between different cell types, chemical components (chemokines) and collagen can be found in [1] and [2], where, respectively, an agent–based and continuum–based formulation is

presented. In this abstract, we summarise some of the results and ideas of our modelling work.

The first class of models is agent–based. Individual cells are treated where cells migrate due to processes like chemotaxis (hence as a result of the gradient of the concentration of a chemical), random walk. We present the description of the two-dimensional case, the three-dimensional case is treated analogously. The cell boundary is divided into nodal points, which are connected by line (boundary) segments (line elements in three dimensions). At the midpoint of each boundary segment, a force is exerted. For classical linear elasticity, where inertia, viscous (damping) effects and plastic effects (permanent deformations) are disregarded, the point forces are treated by a Dirac delta distribution. Let Ω be an open domain with boundary Γ . Suppose that a force \mathbf{F} is exerted at point $\mathbf{x}_i \in \Omega$, then

$$(1) -\nabla \cdot \sigma = \mathbf{F}\delta(\mathbf{x} - \mathbf{x}_i),$$

where $\sigma = 2\mu\varepsilon + \lambda \ (\nabla \cdot \mathbf{u})I$, the strain is given by $\varepsilon = \frac{1}{2}(\nabla \mathbf{u} + \nabla \mathbf{u}^T)$. The fundamental solution in the 2D (infinite) plane is given by

(2)
$$\mathbf{u}(\mathbf{x}) = -\frac{1}{8\pi E(1-\nu)} \left((3-4\nu) \ln(||\mathbf{x} - \mathbf{x}_i||) I + \frac{(\mathbf{x} - \mathbf{x}_i) \otimes (\mathbf{x} - \mathbf{x}_i)}{||\mathbf{x} - \mathbf{x}_i||^2} \right) \mathbf{F},$$

where E and ν , respectively, represent the Young's modulus and Poisson ratio. A 3D counterpart has also been derived. It is easily shown that this expression is not in $H^1(\Omega)$. D'Angelo has proved well-posedness of a Laplace problem with a Dirac delta distribution in weighted Sobolev spaces. We are in the process of demonstrating well-posedness of solutions of the above PDE with appropriate boundary conditions. Since we consider the cell boundary as a (moving) manifold, we sum over all cell boundary points and multiply by the measure (length in 2D and area in 3D) of the boundary element, to get

(3)
$$-\nabla \cdot \sigma = \sum_{i} \mathbf{Q}(\mathbf{x}_{i}) \delta(\mathbf{x} - \mathbf{x}_{i}) \mathbf{n}(\mathbf{x}_{i}) \Delta \Gamma(\mathbf{x}_{i}),$$

where **Q** represents the force per unit of measure. In case of multiple cells, summation over all cells is applied. Using the fundamental solution and superposition (due to linearity of the PDE), one obtains the following solution in the 2D plane

(4)
$$\mathbf{u}(\mathbf{x}) = -\frac{1}{8\pi E(1-\nu)} \sum_{i} \quad \left((3-4\nu) \ln(||\mathbf{x}-\mathbf{x}_{i}||) I + \frac{(\mathbf{x}-\mathbf{x}_{i}) \otimes (\mathbf{x}-\mathbf{x}_{i})}{||\mathbf{x}-\mathbf{x}_{i}||^{2}} \right) \mathbf{Q}(\mathbf{x}_{i}) \mathbf{n}(\mathbf{x}_{i}) \Delta \Gamma(\mathbf{x}_{i}),$$

In [3] regularized Dirac delta distribution by Gaussian functions are considered, as well as consistency and convergence between the regularized and nonregularized distributions.

Since in reality, tissues contain water (blood) to a large extent and since the myofibroblasts release chemicals that change the mechanical properties and structure of collagen, the above formalism is enriched with morphoelasticity, which keeps track of permanent deformations of the tissue. The morphoelastic framework is based on three 'deformation states': the initial state, the current state and

a revised equilibrium state. The difference between the revised equilibrium state and the initial state reflects the permanent displacements and deformation of the tissue. The partial differential equations for morphoelasticity are given by

(5)
$$\rho(\frac{D\mathbf{v}}{Dt} + (\nabla \cdot \mathbf{v})\mathbf{v}) - \nabla \cdot \sigma = \mathbf{F}$$

$$(6) \frac{D\varepsilon}{Dt} + (\nabla \cdot \mathbf{v})\varepsilon + \varepsilon \operatorname{skw}(\nabla \mathbf{v}) - \operatorname{skw}(\nabla \mathbf{v}) \varepsilon + (\operatorname{tr}(\varepsilon) - 1) \operatorname{sym}(\nabla \mathbf{v}) = -G,$$

where \mathbf{v} and ε , respectively, denote the displacement velocity and effective Eulerian strain. The skw(.), sym(.) and tr(.) operators, respectively, denote the skew symmetric of a tensor, symmetric part of a tensor and the trace of a tensor. The above set of PDEs is solved with initial and boundary conditions for \mathbf{v} and an initial condition for ε . The forcing is denoted by F and rate of permanent displacements (and deformations) is quantified by the tensor G. The displacement is obtained by integration of \mathbf{v} over time.

This morphoelasticity formulation is also applied to a full continuum-based model. The continuum-based model involves PDEs for the densities of cells (fibroblasts and myofibroblasts), a chemokine and the density of collagen, as well as the PDEs for morphoelasticity. The model can be found in [2]. The patient–specific nature of many of the input parameters brings in uncertainty in the outcomes. For this reason, a stability analysis [2] and a Bayesian parameter sensitivity analysis for the 1D case has been done [4]. The finite element implementation has been done in 1D and in 2D. In the 2D case, a moving mesh ALE method has been implemented on the basis of linear Lagrangian basis functions. The mesh quality is monitored by checking the angles of the triangles. If the mesh quality is lower than a predefined tolerance, then global remeshing is applied. Using the 2D computational framework, several wound geometries are currently being analysed.

The uncertainty in the modelling framework necessitates interpretation of the modelling outcomes in a statistical sense, where we estimate (posterior) probability distributions on the basis of prior probability distributions for the input parameters. This Bayesian framework is also used for the reproduction of the finite element results by a neural network, which yields very quick estimations of the statistical parameters of interest that can be used by clinicians.

- [1] Q. Peng, F.J. Vermolen, Agent-based modelling and parameter sensitivity analysis with a finite-element method for skin contraction, Biomechanics and Modelling in Mechanobiology, 19 (6) (2020), 2525–2551.
- [2] G. Egberts, F.J. Vermolen, P.P.M. van Zuijlen, Stability of a one-dimensional morphoelastic model for post-burn contraction, Journal of Mathematical Biology 83 (3) (2021), 1–35.
- [3] Q. Peng, F.J. Vermolen, Numerical methods to compute stresses and displacements from cellular forces: Application to the contraction of tissue, Journal of Computational and Applied Mathematics, 404 (2022), 113892.
- [4] G. Egberts, F.J. Vermolen, P.P.M. van Zuijlen, Sensitivity and feasibility of a onedimensional morphoelastic model for post-burn contraction, Biomechanics and Modelling in Mechanobiology, 20 (6) (2021), 2147–2167.

From Micro to Macro: Sediment Transport Simulations with a Fully Resolved Lattice Boltzmann - Discrete Element Method

Christoph Rettinger

(joint work with Ulrich Rüde, Bernhard Vowinckel)

Sediment transport denotes the mobilization of densely packed particles through the action of a flowing fluid in which the sediments are entrained. It, thus, naturally occurs in rivers and seas and is a fascinating geophysical multiscale problem. On the microscale, the onset and characteristics of this movement depend, e.g., on the local flow strength and individual grain properties like size and shape. These features result in a grain-selective transport that becomes visible on the macroscale as bed structures like ripples and dunes and effects like downstream-fining in rivers. As these determine the typical spatial and temporal scales of interest for engineers, corresponding macroscale models have been developed that view the system as two continua, fluid and solid. For a successful application, however, they require closure relations obtained from accurate studies at the microscale.

Simulations that assist this upscaling procedure by providing predictive results have to apply thoroughly validated numerical methods and typically very fine temporal and spatial resolutions to accurately capture all relevant features of the fluid-particle interaction. These simulation requirements result in high computational costs that can only be tackled by high-performance computing (HPC) and specifically designed algorithms. Recently, we developed such a tool for dense particulate flows [5] within the HPC multiphysics framework WALBERLA [2]. It employs the lattice Boltzmann method (LBM) to model the fluid flow above the bed and inside the pores. The discrete element method (DEM) accounts for frictional collisions between particles. The coupling is based on the momentum exchange of both phases, augmented by lubrication correction models to capture strong short-range hydrodynamic interactions between particles. All components work on strictly localized parts of the complete simulation data, making this approach well-suited for massively parallel execution on supercomputers.

Its usefulness in the context of multiscale analysis has recently been demonstrated by deriving a rheological description of sediment bed dynamics [6]. These studies are based on the so-called $\mu(J)$ rheology framework [3], which links the macroscopic friction coefficient μ and the particle volume fraction ϕ to the viscous number J, a non-dimensional measure for the shear rate. In previous laboratory experiments [3, 4], this framework has already been successfully parameterized and applied to describe the behavior of packed beds consisting of monodisperse spheres.

Our simulations studied a similar setup featuring several ten thousand fully resolved particles that initially form a packed bed and are subject to a laminar Couette-type flow. Once a statistically stationary state was observed, we extracted the relevant rheological properties via spatial and temporal averages. We found a close agreement to these experimental results for a monodisperse bed. In particular, we could confirm the so-called creep regime for very low viscous numbers

that was before then only observed by Houssais et al. [4] and was debatable due to possible experimental imperfections. Based on the further evidence from our simulation results, we proposed an extension to the original $\mu(J)$ model to cover this regime as well. The complete model that captures the system's rheological behavior is then given as:

(1)
$$\mu(J) = \underbrace{\mu_0 + \frac{\mu_1 - \mu_0}{1 + J_c/J}}_{\mu^c} + \underbrace{\frac{\mu_2 - \mu_1}{1 + J_f/J}}_{\mu^f} + \underbrace{\frac{5}{2}\phi_m J^{1/2} + J}_{\mu^h},$$

(2)
$$\phi(J) = \frac{\phi_m}{1 + (K_n J)^{1/2}}.$$

The first relation is composed of the hydrodynamic (μ^h) , the frictional (μ^f) , and the newly added creep (μ^c) regime. The model depends on the maximum particle volume fraction ϕ_m and features empirically determined parameters μ_0 , μ_1 , μ_2 , J_c , J_f , and K_n .

Since most sediment beds exhibit differently-sized particles, we carried out simulations of polydisperse setups by sampling the particle diameter from a log-normal distribution with different variance values. We could show that the above rheological relations are equally applicable for these cases, given that the parameters μ_1 , μ_2 , and K_n are adjusted correspondingly. By expressing these parameters as functions of ϕ_m , which increased with the degree of polydispersity and was thus taken as a surrogate to express it, we obtained a general rheology model for polydisperse packings.

These extensions showcased how macroscale models can benefit from simulations at the microscale. For further advances on the modeling side, the proposed generalized parameterization based on ϕ_m as the sole measure for polydispersity should be challenged by considering bimodal or other size distributions. In those cases, the vertical size-based segregation process might need to be addressed explicitly as it continuously changes the local bed composition. This behavior could prevent the formation of a statistically stationary state which is, however, required to extract averaged rheological quantities. Moreover, the effect of particle shape is also largely unknown. Incorporating non-spherical shapes in the microscale simulation leads to additional challenges regarding complex numerical algorithms and their in-depth validation.

Mathematically, an in-depth analysis of the macroscale models is necessary to ensure their stable numerical solution. It has recently been noticed that applying the $\mu(J)$ rheology in granular flow models can result in an ill-posed problem that requires regularization [1]. This issue has to be investigated for the proposed extended rheology model and in the context of two-phase models. Only then do larger systems like rivers become computationally accessible in a robust manner.

References

- T. Barker, J. M. N. T. Gray, Partial regularisation of the incompressible μ(I)-rheology for granular flow, Journal of Fluid Mechanics 828 (2017) 5–32.
- [2] M. Bauer, S. Eibl, C. Godenschwager, N. Kohl, M. Kuron, C. Rettinger, F. Schornbaum, C. Schwarzmeier, D. Thönnes, H. Köstler, U. Rüde, walerla: A block-structured highperformance framework for multiphysics simulations, Comput. Math. Appl. 81 (2021) 478– 501
- [3] F. Boyer, É. Guazzelli, O. Pouliquen, Unifying suspension and granular rheology, Phys. Rev. Lett. 107 (2011) 188301.
- [4] M. Houssais, C. P. Ortiz, D. J. Durian, D. J. Jerolmack, Rheology of sediment transported by a laminar flow, Phys. Rev. E 94 (2016) 062609.
- [5] C. Rettinger, U. Rüde, An efficient four-way coupled lattice Boltzmann discrete element method for fully resolved simulations of particle-laden flows, J. Comput. Phys. 453 (2022) 110942.
- [6] C. Rettinger, S. Eibl, U. Rüde, B. Vowinckel, Rheology of mobile sediment beds in laminar shear flow: effects of creep and polydispersity, J. Fluid Mech. 932 (2022) A1.

Reduced models for multiscale industrial structures : beyond homogeneization

PATRICK LE TALLEC (joint work with Bertrand Leturcq)

In memoriam of Roland Glowinski 1937-2022, great scientist, leader and friend.

Progressive deformation of nuclear fuel assemblies that occurs during a succession of irradiation cycles within a nuclear reactor is at the core of numerous interactions. Its study requires a mechanical model of fuel assemblies, taking into account irradiation growth and creep, the different friction mechanisms within the structure, to be combined to a hydraulic model of the core to address the fluidstructure interaction phenomenology. A multiscale approach is required due to the high complexity of the multi-body multi-physics calculations, which involves something like 4 million contact surfaces and up to sixty thousands fuel rods. In order to improve the representativeness of the core model without penalizing the computational cost of the coupled simulations, model order reduction can be proposed at the scale of each of the 241 fuel assemblies present at the reactor core. It borrows the concepts of the Nonlinear Transformation Field Analysis (NTFA) as used in non-linear homogenization [1]. The theoretical formulations and the application to slender structures with friction and nonlinear creep are discussed below, together with the questions which are left open when trying to give a more theoretical ground to the proposed strategy.

The engineering challenge is to limit the fuel assemblies permanent bows which can be at the origin of costly incidents during the pull out or of poor functioning of the reactor's control safety bars. The phenomena to take into account include the non uniform irradiation growth of the fuel rods, the irradiation creep of the structure, the existence of dry friction forces, and the heterogeneous relaxation of the holding springs. The collective response of the hundreds of fuel assemblies

inside the core couples the global effect of the external loading, the localized creep of the structural elements and the local evolution of the friction force inside each holding spring. The time scale is of the order of one year and corresponds to a reactor loading cycle. The spatial scale ranges from a rod length of 5m to fixing sizes of 1mm. A full model would require more than 200 millions degrees of freedom and a considerable effort in the local integration of creep, contact and friction. Model reduction is thus needed.

The idea herein is to consider a single fuel assembly as the representative volume element (RVE) classically used in multiphase homogeneisation. In this framework, the solution within a RVE in presence of creep and friction is historically obtained by by Transformation Field Analysis (TFA) as introduced by [2] and [3]. In their construction, these authors decide to choose a limited number of phases within the RVE, each nonlinear phase being supposed to be uniform in space. This very crude approximation allows to apply the original constitutive law (creep or friction) to predict the evolution of the constitutive variable inside the phase p (namely the evolution of the irreversible strain field ε_p^{in} for a problem of creep) at the scale of each nonlinear phase. For an RVE with elasticity tensor \mathbf{L} , given history of irreversible strain ε_p^{in} and subjected to a given macro deformation $\bar{\varepsilon}$ imposed in average to the RVE, the resulting stress field to be used in a global equilibrium equation can be explicitly given at all points by

$$\sigma = \mathbf{L} : \mathbf{A} : \bar{\varepsilon} + \sum_{p} \mathbf{L} : (\mathbf{D}_{p} - \mathbf{I}_{p}) \varepsilon_{p}^{in}$$

with localisation and influence tensors \mathbf{A} and \mathbf{D}_p obtained a priori by solving elementary elasticity problems at the scale of the RVE.

The NTFA strategy of [1] proposes a more accurate approximation of the inelastic strain fields ε_p^{in} by replacing the constant fields by a linear expansion on an orthogonal basis of strain modes μ_p obtained at a controlled accuracy by Proper Orthogonal Decomposition (POD) based on a collection of precomputed snapshots. The challenge is then to project the nonlinear constitutive law on these modes without using local integration on each RVE and at each time step, which would be of the same complexity as the original multiscale problem. A simple but efficient averaging rule is proposed in [1] for constitutive laws based on a nonlinear dissipation potential controlled by the local Von Mises equivalent stress σ_{eq}

$$\dot{\varepsilon}_{p}^{in} := \frac{1}{V} \int_{V} \dot{\varepsilon}^{in} : \mu_{p} dV = \frac{1}{V} \int_{V} \frac{3}{2} \frac{\partial \psi}{\partial \sigma_{eq}} (\sigma_{eq}) \frac{\sigma' : \mu_{p}}{\sigma_{eq}} dV
\approx \frac{1}{V} \frac{3}{2s_{r}} \frac{\partial \psi}{\partial \sigma_{eq}} (s_{r}) \int_{V} \sigma' : \mu_{p} dV$$

with $s_r^2 = \langle \sigma_{eq}^2 \rangle$ the volume average of the square of the local Von Mises equivalent stress. The above integral is a linear combination of a small number of precomputed dissipation integrals. The function s_r^2 is a quadratic function of the stress field, hence reduces to a quadratic form directly computed in terms of modes with no need of an element wise integration of the detailed model at each time step. This results in a considerable gain of computing time and turns out to be

very efficient for mildly nonlinear creep. It can be generalized to situations with space variable coefficients or involving more complex anisotropic laws [4] .

Extending this approach to nonlinear industrial structures requires two additional ingredients in order to extend the notion of imposed deformation to a complex substructure and to build a sign preserving modal expansion of the contact forces. For the first point, we use a domain decomposition strategy. A substructure like a fuel assembly is a natural subdomain of the full structure, and its motion can be accurately controlled by the rigid body motions of each of its interface with the global structure. In this framework, the "global deformation" of a single fuel assembly is defined by the three translational modes of each of its 11 spacing grids.

The modal expansion of the contact forces uses a positive decomposition of contact forces snapshots X on r positive modes using a Non negative Matrix Factorisation $X \approx \hat{\Lambda} H$ obtained by least squares minimization of the approximation error using alternating directions. The result is a modal matrix $\hat{\Lambda}$ of r positive columns (typically $r \approx 10$). The local contact conditions are then transferred to the reduced model through a simple projection of the contact constraints on these positive modes. Last, a modal basis of slip displacements is obtained by POD, to be combined to averaged stick slip criteria written at mode level.

Altogether, the reduced model uses the full elastic problem but with a reduced nonlinear loading, based on simplified boundary conditions, reduced creep laws (as in standard NTFA) to get the evolution of the creeping modes, reduced (NMF projected) contact conditions to get the reduced normal forces, and a NTFA like reduced friction law to get the evolution of each slipping mode. With this loading reduction, the local solution can be explicitly obtained from a small set of precomputed elementary elastic solutions. The numerical tests indicate that considerable cost reduction (a factor of 20 to 100) can be achieved while preserving engineering accuracy.

The proposed strategy is quite general. It embeds an error control in the modal construction of the boundary displacements and of the creep modes. The open problems concern on one hand the error analysis of the NTFA averaged material law and on the other hand the combined control of the modal expansion of the contact forces and of the slipping modes in order to improve robustness and accuracy.

- [1] J.C. Michel, P. Suquet, Nonuniform transformation field analysis., Int. J. Solids Struct. 40, (2003), 6937–6955.
- [2] G.J. Dvorak, Transformation field analysis of inelastic composite materials. Proc. R. Soc. Lond. Ser. Math. Phys. Sci. 437, (1992), 311–327.
- [3] J. Fish, K. Shek Finite deformation plasticity for composite structures: Computational models and adaptive strategies., Comput. Methods Appl. Mech. Eng. 172, (1999), 145–174.
- [4] J.C. Michel, P. Suquet, A model-reduction approach to the micromechanical analysis of polycrystalline materials. Comput. Mech. 57, (2016), 483-508.

Participants

Dr. Josefin Ahlkrona

Matematiska Institutionen Stockholms Universitet 10691 Stockholm SWEDEN

Dr. Azhar Alhammali

College of Applied Studies & Community Service, Imam Abdulrahman Bin Faisal University King Faisal Road P.O. Box P.O Box: 1982. 34212 Dammam SAUDI ARABIA

Prof. Dr. Paola F. Antonietti

MOX-Laboratory for Modeling and Scientific Computing Dipartimento di Matematica Politecnico di Milano Piazza Leonardo da Vinci 32 20133 Milano ITALY

Prof. Dr. Ferdinando Auricchio

Dip Ingegneria Civile e Architettura Universita di Pavia Via Ferrata 3 27100 Pavia ITALY

Jonas Beddrich

Zentrum Mathematik TU München Boltzmannstr. 3 85748 Garching bei München GERMANY

Dr. Lorena Bociu

Department of Mathematics North Carolina State University Campus Box 8205 Raleigh NC 27695-8205 UNITED STATES

Prof. Dr. Susanne C. Brenner

Department of Mathematics Louisiana State University 303 Lockett Hall Baton Rouge LA 70803-4918 UNITED STATES

Dr. Carina Bringedal

University Stuttgart Institute for Modelling Hydraulic and Environmental Systems Pfaffenwaldring 61 70569 Stuttgart GERMANY

Prof. Dr. Martina Bukač

Applied and Computational Mathematics and Statistics University of Notre Dame Notre Dame, IN 46556-5683 UNITED STATES

Prof. Dr. Suncica Canic

Department of Mathematics University of California, Berkeley 911 Evans Hall Berkeley CA 94720-3860 UNITED STATES

Prof. Dr. Eric T. Chung

Department of Mathematics The Chinese University of Hong Kong Room 220, Lady Shaw Building Shatin, N.T., Hong Kong SAR CHINA

Prof. Dr. Clint Dawson

Oden Institute for Computational Engineering and Sciences (ICES) University of Texas at Austin 201 E. 24th St, Stop C0200 Austin, TX 78712-1085 UNITED STATES

Prof. Dr. Laura De Lorenzis

CLA J 13

Department of Mechanical and Process Engineering ETH Zürich Tannenstrasse 3 8092 Zürich SWITZERLAND

Prof. Dr. Alexander Düster

Numerische Strukturanalyse mit Anwendungen in der Schiffstechnik Institut für Konstruktion und Festigkeit von Schiffen Technische Universität Hamburg Am Schwarzenberg-Campus 4 (C) 21073 Hamburg GERMANY

Tobias Duswald

CERN Organisation Europeenne pour la Recherche Nucleaire 1211 Genève 23 SWITZERLAND

Dr. Markus Gahn

Interdisziplinäres Zentrum für wissenschaftliches Rechnen (IWR) Universität Heidelberg Im Neuenheimer Feld 205 69120 Heidelberg GERMANY

Dr. Maria Gokieli

Faculty of Mathematics and Natural Sciences Cardinal Stefan Wyszynski University, Warsaw Woycickiego 1/3 01-938 Warszawa POLAND

Prof. Dr. Kenneth M. Golden

University of Utah Department of Mathematics 155 South 1400 East, RM 233 Salt Lake City, UT 84112-0090 UNITED STATES

Dr. Giovanna Guidoboni

Department of Electrical Engineering and Computer Science, Department of Mathematics University of Missouri-Columbia Columbia, MO 65211-4100 UNITED STATES

Gladys Gutierrez Lupinta

Zentrum Mathematik TU München Boltzmannstr. 3 85748 Garching bei München GERMANY

Dr. Thi-Thao-Phuong Hoang

Department of Mathematics and Statistics Auburn University Auburn, AL 36849 UNITED STATES

Prof. Dr. Jacques Huyghe

Dept. of Mathematics and Statistics University of Limerick Limerick IRELAND

Assoc. Prof. Dr. Kundan Kumar

Department of Mathematics University of Bergen P.O. Box 7800 5020 Bergen NORWAY

Prof. Dr. Anita Layton

Dept. of Applied Mathematics and Computer Science University of Waterloo Waterloo ON N2L 3G1 CANADA

Prof. Dr. Patrick Le Tallec

Laboratoire Mécanique des Solides École Polytechnique 91128 Palaiseau Cedex FRANCE

Stephan Benjamin Lunowa

Hasselt University
Faculty of Sciences
Computational Mathematics Group
Agoralaan Building D
3590 Diepenbeek
BELGIUM

Dr. Koondanibha Mitra

Mathematisch Instituut Radboud Universiteit Nijmegen Heyendaalseweg 6525 AJ Nijmegen NETHERLANDS

Natalia Nebulishvili

Fakultät für Mathematik Technische Universität München Boltzmannstraße 3 85748 Garching bei München GERMANY

PD Dr. Maria Neuss-Radu

Department Mathematik Friedrich-Alexander-Universität Erlangen-Nürnberg Cauerstraße 11 91058 Erlangen GERMANY

Prof. Dr. Jan Martin Nordbotten

Department of Mathematics University of Bergen P.O. Box Postboks 7803 5020 Bergen NORWAY

Dr. Alice Peng

Mathematisch Instituut Universiteit Leiden Snellius building, Niels Bohrweg 1 P.O. Box Postbus 9512 2333CA Leiden NETHERLANDS

Prof. Dr. Malgorzata Peszynska

Department of Mathematics Oregon State University Kidder Hall 368 Corvallis OR 97331-4605 UNITED STATES

Prof. Dr. Sara Pollock

Department of Mathematics University of Florida 358 Little Hall P.O. Box P.O.Box 118105 Gainesville, FL 32611-8105 UNITED STATES

Prof. Dr. Iuliu Sorin Pop

Hasselt University Faculty of Sciences Agoralaan, Building D Diepenbeek 3590 BELGIUM

Prof. Dr. Alexander Popp

Institut für Mathematik und Computergestützte Simulation Universität der Bundeswehr München Werner-Heisenberg-Weg 39 85577 Neubiberg GERMANY

Prof. Dr. Florin Adrian Radu

Department of Mathematics University of Bergen Postboks 7803 5020 Bergen NORWAY

Prof. Dr. Ernst Rank

TUM Institute for Advanced Study TU München Arcisstr. 21 80290 München GERMANY

Prof. Dr. Alessandro Reali

Department of Civil Engineering and Architecture University of Pavia Via Ferrata, 3 27100 Pavia ITALY

Christoph Rettinger

Chair for System Simulation Friedrich-Alexander-Universität Erlangen-Nürnberg Cauerstr. 11 91058 Erlangen GERMANY

Prof. Dr. Beatrice Riviere

Dept. of Computational & Applied Mathematics Rice University 6100 Main Street Houston, TX 77005-1827 UNITED STATES

Dr. Carmen Rodrigo Cardiel

Departamento de Matematicas Universidad de Zaragoza Edificio de Matemáticas, planta 1 Pedro Cerbuna, 12 50009 Zaragoza SPAIN

Prof. Dr. Tina Roose

Bioengineering Sciences Research Group Faculty of Engineering and Environment University of Southampton University Road Southampton SO17 1BJ UNITED KINGDOM

Assoc. Prof. Dr. Ricardo Ruiz Baier

School of Mathematics Monash University Clayton Victoria 3800 AUSTRALIA

Prof. Dr. Riccardo Sacco

Dipartimento di Matematica Politecnico di Milano Piazza Leonardo da Vinci, 32 20133 Milano ITALY

Prof. Dr. Adelia Sequeira

Departamento de Matematica Instituto Superior Tecnico Avenida Rovisco Pais, 1 Lisboa 1049-001 PORTUGAL

Prof. Dr. Ralph E. Showalter

Department of Mathematics Oregon State University Kidder Hall 368 Corvallis, OR 97331-4605 UNITED STATES

Prof. Dr. John Stockie

Department of Mathematics Simon Fraser University 8888 University Drive, Math Dept. Burnaby BC V5A 1S6 CANADA

Erlend Storvik

Department of Mathematics University of Bergen Allégaten 41 5008 Bergen NORWAY

Prof. Dr. Shuyu Sun

4700 King Abdullah University of Science and Technology (KAUST) Mathematical & Computer Sciences P.O. Box 2360 Jeddah SAUDI ARABIA

Dr. Dumitru Trucu

Department of Mathematics University of Dundee Fulton Building DD1 4HN Dundee DD1 4HN UNITED KINGDOM

Prof. Dr. E. Harald van Brummelen

Faculty of Mechanical Engineering Eindhoven University of Technology Den Dolech 2 P. O. Box 513 5600 MB Eindhoven NETHERLANDS

Prof. Dr. Alessandro Veneziani

Dept. of Mathematics and Computer Science Emory University 400, Dowman Dr. Atlanta, GA 30322 UNITED STATES

Dr. Fred Vermolen

Department WNI Hasselt University Agoralaan D P.O. Box 3590 3590 Diepenbeek BELGIUM

Mr. Naren Vohra

Department of Mathematics Oregon State University Kidder Hall 368 Corvallis, OR 97331-4605 UNITED STATES

Prof. Dr. Thomas Wick

Institut für Angewandte Mathematik Leibniz Universität Hannover Welfengarten 1 30167 Hannover GERMANY

Prof. Dr. Christian Wieners

Fakultät für Mathematik Institut für Angewandte und Numerische Mathematik Karlsruher Institut für Technologie (KIT) Englerstraße 2 76131 Karlsruhe GERMANY

Prof. Dr. Barbara Wohlmuth

Zentrum für Mathematik Technische Universität München Boltzmannstraße 3 85748 Garching bei München GERMANY

Prof. Dr. Zohar Yosibash

Tel Aviv University School of Mechanical Engineering Levanon st 6997801 Ramat Aviv, Tel Aviv 6997801 ISRAEL

Prof. Dr. Ivan Yotov

Department of Mathematics University of Pittsburgh 301 Thackery Hall Pittsburgh, PA 15260 UNITED STATES

Prof. Dr. Yongjie Jessica Zhang

Department of Mechanical Engineering Carnegie Mellon University 1315 Wean Hall 5000 Forbes Avenue 15213 Pittsburgh, PA 15213-3890 UNITED STATES